WNK1-dependent water influx is required for CD4$^+$ T cell activation and T cell-dependent antibody responses

Joshua Biggs O'May[1], Lesley Vanes[1], Leonard L. de Boer[1,2], Harald Hartweger[1], Simone Kunzelmann[1], Darryl Hayward[1], Miriam Llorian[1], David A. Lewis[1], Robert Köchl[1], Victor L. J. Tybulewicz[1]*

[1]The Francis Crick Institute, London, NW1 1AT, UK
[2]Imperial College, London W12 0NN, UK

*Correspondence to:

Victor L. J. Tybulewicz
The Francis Crick Institute,
1 Midland Road,
London, NW1 1AT, UK

Tel: +44 20 3796 1612
Email: Victor.T@crick.ac.uk

Present addresses:

JBOM: joshua.biggsomay@gmail.com
LLdB: Science for Life Laboratory, Department of Women's and Children's Health, Karolinska Institute, Box 1031, SE-171 21 Solna, Sweden
HH: Laboratory of Molecular Immunology, The Rockefeller University, 10065 New York, NY, USA
DH: GSK, Stevenage, SG1 2NY, UK
RK: Kings College London, London, SE1 9RT, UK

Abstract

Signaling from the T cell antigen receptor (TCR) on $CD4^+$ T cells plays a critical role in adaptive immune responses by inducing T cell activation, proliferation, and differentiation. We demonstrate that WNK1, a kinase implicated in osmoregulation in the kidney, is required in T cells to support T-dependent antibody responses. WNK1-deficient $CD4^+$ T cells are severely impaired in their ability to proliferate and to generate antigen-specific T follicular helper cells in response to immunization with a T-dependent antigen. We show that WNK1 and its downstream OXSR1 and STK39 kinases are required for TCR signaling in $CD4^+$ T cells and for entry into cell cycle. Additionally, by preventing ATR activation, this pathway is required for T cells to progress from G2 into M phase of the cell cycle. Unexpectedly, we show that this WNK1 pathway regulates water influx, most likely through AQP3, which is required for TCR-induced signaling and cell cycle entry. Thus, TCR signaling via WNK1, OXSR1, STK39 and AQP3 leads to water entry that is essential for $CD4^+$ T cell proliferation and hence T cell-dependent antibody responses. Given the broad expression of WNK1, WNK1-dependent water influx may be a common feature of mitogenic pathways in many cell types, both within the immune system and beyond.

One Sentence Summary

T cell antigen receptor signaling via the WNK1 kinase causes water entry which is essential for $CD4^+$ T cell proliferation.

Keywords

T cell activation, T cell antigen receptor, TCR signaling, WNK1, OXSR1, STK39, aquaporin, water flux, ATR.

INTRODUCTION

T cell activation is a critical event in the initiation of T cell-dependent (TD) immune responses. To generate TD antibody responses, naive $CD4^+$ T cells circulate through lymphoid organs scanning peptides presented on MHC class II molecules (pMHCII) on the surface of antigen-presenting cells (APC)[1]. Simultaneous binding of cognate pMHCII complexes to the T cell antigen receptor (TCR) and ligation of costimulatory receptors such as CD28 results in biochemical signals leading to LFA-1 integrin-mediated adhesion of the T cell to the APC, and subsequent activation of the T cell characterized by changes in gene expression, cytokine secretion, cell division and differentiation into effector T cells such as T follicular helper (T_{FH}) cells[2]. T_{FH} cells provide help to antigen-specific B cells, supporting their continued activation, proliferation, and differentiation into antibody-secreting plasma cells, thereby generating an antibody response.

WNK1 has been studied most extensively in the kidney where it acts in epithelial cells of the distal tubules to regulate uptake of ions from urine into the blood stream[3,4]. WNK1 phosphorylates and activates OXSR1 and STK39, two related kinases, which in turn phosphorylate members of the electroneutral SLC12A-family of ion co-transporters, leading to the net influx of Na^+, K^+ and Cl^- ions[5-8]. This WNK-induced ion influx in turn leads to passive water influx, which underlies the role of WNK1 in regulating cell volume[4,9].

Our previous studies in $CD4^+$ T cells showed that signaling from the TCR and from the CCR7 chemokine receptor acting via phosphatidylinositol 3-kinase leads to rapid activation of WNK1[10]. Furthermore, we found that WNK1 regulates both adhesion and migration of T cells. WNK1 is a negative regulator of TCR- and CCR7-induced adhesion through the LFA-1 integrin. Conversely, WNK1 is a positive regulator of CCR7-induced T cell migration. CCL21 binding to CCR7 results in signaling via WNK1, OXSR1, STK39 and

SLC12A2 which is required for migration. In view of the importance of adhesion and migration for T cell activation, we hypothesized that WNK1 may have a critical role in T cells during TD immune responses.

Here we show that WNK1-deficient T cells are unable to support a TD antibody response. Surprisingly, we find that in addition to its role in T cell adhesion and migration, WNK1 is required for TCR/CD28-induced activation. We show that in $CD4^+$ T cells, TCR signaling via WNK1, OXSR1 and STK39 leads to water influx, most likely through AQP3, and that this water influx is required for early TCR signaling and cell cycle progression. Furthermore, WNK1-OXSR1-STK39-AQP3 signaling is required to prevent an ATR-dependent cell cycle arrest at G2. Thus, TCR signaling via WNK1, OXSR1, STK39 leads to water entry via AQP3 which is required for T cell proliferation and TD antibody responses.

RESULTS

WNK1 is essential for the generation of T_{FH} cells and class-switched antibody responses

To investigate if WNK1 is required in T cells for TD immune responses, we inducibly inactivated the *Wnk1* gene in mature T cells, since WNK1 is required for T cell development in the thymus[11]. Using mice with a loxP-flanked allele of *Wnk1* (*Wnk1*^{fl})[12] crossed to mice with a loss of function *Wnk1* allele (*Wnk1*$^{-}$)[10] and mice with a tamoxifen-inducible Cre recombinase expressed from the ROSA26 locus (*ROSA26*^{CreERT2}, RCE)[13], we generated *Wnk1*$^{fl/-}$RCE mice and control *Wnk1*$^{fl/+}$RCE mice. Bone marrow from these two mouse strains was used to reconstitute irradiated RAG1-deficient mice, and 8 weeks later treatment with tamoxifen resulted in the generation of WNK1-deficient (*Wnk1*$^{-/-}$RCE) and control WNK1-expressing (*Wnk1*$^{+/-}$RCE) T cells (Supplementary Figure 1A). *Wnk1*

was efficiently deleted in $CD4^+$ T cells from these chimeras following tamoxifen administration (Supplementary Figure 1B). Importantly, loss of WNK1 did not result in compensatory increase in expression of *Wnk2*, *Wnk3*, or *Wnk4* as measured by RNA sequencing (Supplementary Figure 1C). Thus, *Wnk1*$^{-/-}$RCE $CD4^+$ T cells lack expression of wild-type forms of all *Wnk*-family genes. Using mixed bone marrow chimeras in which *Wnk1* was deleted from all αβT cells, while other cell types retained *Wnk1* expression, we found that following immunization with NP-CGG in alum, the mice failed to generate NP-specific IgG1 antibodies, a hallmark TD response (Figure 1A-B). Thus, WNK1 is required in αβT cells for TD antibody responses.

To identify the WNK1-dependent processes contributing to TD antibody responses, we generated *Wnk1*$^{fl/+}$RCE OT-II and *Wnk1*$^{fl/-}$RCE OT-II bone marrow chimeras which express a TCR (OT-II) specific for an ovalbumin peptide ($OVA_{323-339}$) presented on the I-A^b MHC class II molecule[14]. We treated the chimeras with tamoxifen, isolated WNK1-expressing and WNK1-deficient $CD4^+$ OT-II T cells and transferred these into congenically-marked wild-type (WT) mice which were immunized with ovalbumin (Figure 1C). Flow cytometric analysis showed that WNK1-deficient OT-II T cells were severely impaired in proliferation at day 3, and at day 7 many fewer WNK1-deficient OT-II T cells were recovered compared to controls, and in particular there were very few T_{FH} cells (Figure 1D-J). The almost complete absence of T_{FH} cells likely explains the impaired TD antibody response in mice with WNK1-deficient T cells.

WNK1, OXSR1 and STK39 are required for TCR-induced proliferation of $CD4^+$ T cells

This defect could be due to altered T cell adhesion or migration. Alternatively, since TCR signaling activates WNK1, the kinase could play a direct role in TCR-induced activation.

To study this possibility, we investigated whether the activation defect of WNK1-deficient T cells could be recapitulated *in vitro*. We cultured WNK1-expressing and WNK1-deficient $CD4^+$ OT-II T cells with bone marrow-derived APCs and different doses of $OVA_{323-339}$ peptide (Supplementary Figure 2A). We found that in the absence of WNK1, OT-II T cells were impaired in proliferation, similar to the phenotype observed *in vivo* (Figure 2A-B). Since in this T cell:APC co-culture assay T cells need to adhere to APCs and receive signals from multiple cell surface proteins in addition to the TCR, we simplified the *in vitro* analysis further by activating purified naive $CD4^+$ T cells with plate-bound anti-CD3ε and anti-CD28 antibodies to stimulate the TCR and CD28 respectively (Supplementary Figure 2B). Once again, we found that WNK1-deficient T cells were severely impaired in TCR/CD28-induced proliferation (Figure 2C-D). This observation suggests that the requirement for WNK1 during $CD4^+$ T cell activation is independent of its role in migration and integrin-mediated adhesion as T cells do not need to migrate or adhere to APCs in order to be activated in this experimental system. Our results show that WNK1 is required for TCR/CD28-induced proliferation, explaining the strongly impaired $CD4^+$ T cell expansion *in vivo* during a TD immune response.

To evaluate the role of WNK1 kinase activity in this process, we analyzed TCR/CD28-induced activation of $CD4^+$ T cells expressing a kinase-inactive allele of WNK1 (*Wnk1*^{D368A})[10], a mutation that has been shown to eliminate kinase activity (Supplementary Figure 2B)[7]. Once again, T cells expressing WNK1-D368A showed strongly decreased cell division, similar to the phenotype of WNK1-deficient T cells (Figure 2E-F). To address whether the phenotypic changes observed were due to adaptation of cells to the chronic absence of WNK1 activity, rather than a requirement for WNK1 during TCR stimulation, we made use of WNK463 (WNKi), a highly selective WNK kinase inhibitor[15]. Activation of WT $CD4^+$ T cells in the presence of WNKi showed that acute inhibition of WNK1, the only

WNK-family kinase expressed in T cells (Supplementary Figure 1C), resulted once again in dramatically impaired proliferation upon TCR and CD28 co-stimulation (Supplementary Figure 2C, Figure 2G-H). Taken together, these results show that WNK1 kinase activity is required for TCR/CD28-induced proliferation of $CD4^+$ T cells.

The best characterized WNK1 substrates are the related OXSR1 and STK39 kinases[5-8]. Stimulation of $CD4^+$ T cells through the TCR and CD28 resulted in an increase in phosphorylation of OXSR1 on Ser325, a site phosphorylated by WNK1[7] (Supplementary Figure 3A). Treatment with WNKi caused a strong reduction in this phosphorylation, demonstrating that WNK1 kinase activity is required both for TCR-CD28-induced and basal phosphorylation of OXSR1. Thus, we investigated if these proteins might be important for WNK1-dependent T cell activation. We again used mice with a loxP-flanked allele of *Oxsr1* (*Oxsr1*^{fl}), which could be inducibly deleted by tamoxifen treatment. To account for potential redundancy between OXSR1 and STK39, we crossed in the *Stk39*^{T243A} allele which expresses an STK39 mutant that cannot be phosphorylated and activated by WNK1[16]. We used bone marrow from *Oxsr1*$^{fl/fl}$*Stk39*$^{T243A/T243A}$RCE as well as control *Oxsr1*$^{+/+}$*Stk39*$^{+/+}$RCE mice to reconstitute irradiated RAG1-deficient mice (Supplementary Figure 3B). OXSR1 was efficiently deleted in mature $CD4^+$ T cells from these chimeras following tamoxifen administration (Supplementary Figure 3C). *Oxsr1*$^{-/-}$ *Stk39*$^{T243A/T243A}$RCE double mutant $CD4^+$ T cells exhibited reduced TCR/CD28-induced proliferation, however, the decrease was smaller than that seen in the absence of WNK1 (Figure 2I-J). Our results suggest that a WNK1-OXSR1-STK39 pathway is required for $CD4^+$ T cell proliferation.

The WNK1 pathway is required for progression through the cell cycle

To gain a better understanding of how the WNK1 pathway impacts on T cell proliferation, we evaluated how the cells progress through the cell cycle in the absence of WNK1. Ki67 expression is induced as cells progress from G0 to G1 phase of the cell cycle. Following TCR/CD28 stimulation, WNK1-deficient T cells upregulated Ki67 more slowly than control cells, indicating that their entrance into the cell cycle is delayed (Figure 3A). Analysis of Ki67+ cells 3 days after the start of TCR/CD28 stimulation showed that an increased fraction of WNK1-deficient cells accumulated in the G2 phase relative to controls (Figure 3B-C, Supplementary Figure 4A), suggesting that their reduced rate of proliferation may also be due to slower progression through G2 or arrest at the G2/M checkpoint. Furthermore, the rate of incorporation of the nucleoside analog EdU was greatly reduced in WNK1-deficient T cells indicating that DNA replication and progression through S phase is also severely hampered in the absence of WNK1 (Figure 3D-E).

In response to TCR/CD28 co-stimulation, *Oxsr1*$^{-/-}$*Stk39*$^{T243A/T243A}$RCE double mutant T cells also upregulated Ki67 more slowly than control cells, accumulated in S and G2 phases of the cell cycle and had reduced rates of EdU incorporation (Figure 3F-J, Supplementary Figure 4B). Thus WNK1, OXSR1 and STK39 are required for CD4^{+} T cells to efficiently exit G0, progress through S and G2.

The WNK1 pathway is required for early TCR signaling

The defect in G0 exit in TCR/CD28-stimulated WNK1-deficient T cells could be caused by alterations in early signaling events triggered following engagement of TCR and CD28, which provide the mitogenic signals in our system. Flow cytometric analysis of CD4^{+} T cells stimulated with anti-CD3ε and anti-CD28 antibodies in solution showed that WNK1 inhibition had no effect on the phosphorylation of the CD3ζ component of the TCR (p-

CD3ζ), one of the earliest measurable biochemical changes following TCR stimulation (Figure 4A, Supplementary Figure 5A). As expected, this TCR/CD28-induced increase in p-CD3ζ was blocked by treatment with a SRC kinase inhibitor (SRCi). In contrast, WNKi treatment caused a significant reduction in the phosphorylation of the ZAP70 kinase (p-ZAP70) and the ERK kinases (p-ERK), both of which were also blocked by SRCi (Figure 4B-C, Supplementary Figure 5B-C). Moreover, p-ERK was reduced in WNKi-treated $CD4^+$ T cells activated by plate-bound anti-CD3ε and anti-CD28 antibodies for 1 h, conditions that result in biphasic activation of ERK and T cell proliferation (Figure 4D, Supplementary Figure 5D)[17]. A similar decrease in TCR/CD28-stimulated p-ERK was also seen in *Oxsr1*$^{-/-}$*Stk39*$^{T243A/T243A}$RCE T cells (Figure 4E, Supplementary Figure 5E), implying that WNK1-OXSR1-STK39 signaling is required for TCR/CD28-induced p-ERK.

Defects in the WNK1 pathway result in an ATR-dependent cell cycle arrest in G2

Accumulation of cells in G2 could be caused by the triggering of a cell cycle checkpoint, for example through activation of the ATM or ATR kinases in response to DNA damage. Immunoblot analysis of phosphorylated RPA32 (S4/8, p-RPA32) and phosphorylated H2AX (S139, γH2AX), markers of single-stranded and double-stranded DNA damage respectively, showed no significant elevation of either in WNK1-inhibited T cells stimulated through the TCR and CD28 (Supplementary Figure 4C-D). However, as expected, both were robustly increased by treatment with hydroxyurea, which causes replication fork stalling and subsequent DNA damage. Since γH2AX is a marker of ATM activity, these results imply that inhibition of WNK1 does not result in ATM activation. To measure ATR activity, we immunoblotted cell extracts for phosphorylated CHK1 (S345, p-CHK1), a product of ATR activity. Unexpectedly, we detected elevated p-CHK1 in TCR/CD28-stimulated WNKi-treated T cells compared to control T cells, which was reduced in cells

treated with AZD6738, an ATR inhibitor (ATRi), indicating that ATR activity was increased in the absence of WNK1 activity (Figure 4F). Extending this analysis, we found a similar increase in ATR activity in TCR/CD28-stimulated *Oxsr1*$^{-/-}$*Stk39*$^{T243A/T243A}$RCE T cells (Figure 4G). To evaluate if increased ATR activity in WNK1-inihibited T cells was causing cell cycle arrest, we activated WNK1-inihibited T cells and treated them with ATRi. We found that the inhibitor significantly reduced the fraction of cells in G2, implying that the block in G2 is predominantly due to ATR activation (Figure 4H, Supplementary Figure 4E). Thus, compromised TCR/CD28 signaling via WNK1, OXSR1 and STK39 leads to ATR activation and cell cycle arrest.

Na^+ and Cl^- ions are important for TCR/CD28-induced ERK activation

In kidney epithelial cells, signaling through WNK1, OXSR1 and STK39 leads to phosphorylation of SLC12A-family ion co-transporters and net influx of Na^+, K^+ and Cl^- ions[6]. Thus, we hypothesized that TCR signaling via the WNK1-OXSR1-STK39 pathway leads to SLC12A-dependent ion influx which is required for T cell activation. In support of this, we found that reducing the concentration of Na^+ and Cl^- ions while maintaining isotonicity with L-glucose, an inert osmolyte, impaired TCR-CD28-stimulated p-ERK in $CD4^+$ T cells (Figure 5A). Furthermore, replacement of Cl^- ions in the medium with gluconate, also strongly reduced TCR/CD28-induced p-ERK (Figure 5B). Taken together, these results imply that Na^+ and Cl^- ions are likely important for TCR/CD28 signaling independently of their effect on osmolarity.

To examine the role of the SLC12A-family ion co-transporters in this process, we initially investigated their expression in T cells. RNA sequencing showed that of the 9 family members, 5 were expressed in mouse $CD4^+$ T cells: *Slc12a2*, *Slc12a4*, *Slc12a6*, *Slc12a7* and *Slc12a9* (Figure 5C). Furthermore, flow cytometric analysis showed that TCR/CD28

stimulation resulted in increased phosphorylation of SLC12A2 on Thr203, Thr207 and Thr212, sites that are phosphorylated by OXSR1 and STK39[8] (Figure 5D, Supplementary Figure 6A). Treatment of $CD4^+$ T cells with WNKi resulted in decreased phosphorylation of SLC12A2, in support of the hypothesis that a WNK1-OXSR1-STK39 pathway leads to SLC12A2 phosphorylation in T cells. To investigate the role of SLC12A2 in T cell activation we made use of bumetanide, an SLC12A2 inhibitor (SLC12A2i) which we had previously shown inhibits mouse $CD4^+$ T cell migration[10,18], and also examined SLC12A2-deficient T cells. We found that treatment with SLC12A2i or loss of SLC12A2 did not affect TCR-CD28-induced p-ERK or the percentage of $CD4^+$ T cells that divided at least once (Supplementary Figure 6B-E).

Since SLC12A2 is only one of 5 SLC12A-family members that is expressed in T cells, several of which are known substrates of the WNK1-OXSR1-STK39 pathway[4], other SLC12A members may be more important than SLC12A2 in transducing WNK1 pathway signals that regulate T cell activation and proliferation. Despite their structural similarity, the family members have different, opposing functions. While WNK1-OXSR1-STK39-induced phosphorylation of SLC12A2 (NKCC1) leads to its activation and hence influx of Na^+, K^+ and Cl^- ions, phosphorylation of SLC12A6 (KCC3) or SLC12A7 (KCC4) inhibits these transporters, blocking efflux of K^+ and Cl^- ions, with the net result being an increase in the intracellular concentrations of Na^+, K^+ and Cl^- ions[5]. Bearing in mind this complication, we examined the effect of DIOA, an inhibitor of SLC12A6 and SLC12A7 (SLC12A6/7i) on T cell activation. Once again, we found that treatment of T cells with SLC12A6/7i did not affect TCR/CD28-induced p-ERK or cell division, possibly because the inhibitor is simply reinforcing their physiological inhibition by WNK1 activity downstream of the TCR (Supplementary Figure 6B-E). Taken together, these results

indicate that Na^+ and Cl^- ions are important for TCR/CD28-induced T cell activation, but we were unable to establish if this was due to a role for SLC12A-mediated ion influx.

AQP3 is required for TCR-induced proliferation

One of the effects of ion influx into the cell is that the resulting osmotic gradient causes passive water influx. Indeed, WNK1 plays an important role in the osmoregulation of cells and in modulating cell volume by regulating ion influx and consequent osmotically-driven water influx[9]. Thus, we hypothesized that TCR signaling through WNK1 would result in water influx and that this may be required for T cell activation. In support of this, stimulation of WT naive $CD4^+$ T cells with anti-CD3ε and anti-CD28 resulted in a cell volume increase as measured using a Casy® cell counter, whereas WNKi-treated cells were smaller and did not increase in volume to the same extent (Figure 6A). We extended this analysis by directly measuring the volume of the cells by super-resolution microscopy. This showed that TCR/CD28 stimulation resulted in an ~11% increase in cell volume, whereas WNKi treatment reduced basal cell volume by ~22% and eliminated the TCR-induced increase in volume (Figure 6B, C). In contrast, treatment of $CD4^+$ T cells with SLC12A2i did not affect basal or TCR/CD28-induced volume, in agreement with the lack of effect of this inhibitor on TCR-induced p-ERK and proliferation (Supplementary Figure 6F). Thus, WNK1 is required for cell volume increase in response to TCR and CD28 stimulation, consistent with our hypothesis that TCR signaling via WNK1 results in water influx.

Water entry into mammalian cells is mediated by aquaporins, channels that allow water to passively flow into or out of cells in response to an osmotic gradient[19]. RNA sequencing analysis showed that of the 11 functional aquaporin genes in mice, $CD4^+$ T cells express detectable levels of only three family members: *Aqp3*, *Aqp9* and *Aqp11* (Figure 6D). Since of these three, *Aqp3* is expressed at the highest level, we decided to use DFP00173, an

AQP3 inhibitor (AQP3i)[20], to test the requirement for water entry in T cell activation. As expected, AQP3i reduced the water permeability of $CD4^+$ T cells (Figure 6E). Notably, treatment of naive $CD4^+$ T cells with AQP3i gave a significant reduction in cell proliferation (Figure 6F-G). Furthermore, AQP3i treatment also resulted in reduced TCR/CD28-induced p-ERK induction following 1 h of stimulation, as well as increased p-CHK1 after 3 d of stimulation (Figure 4D, F), similar to the phenotype caused by inhibition or mutation of WNK1, OXSR1 and STK39.

In addition to water, AQP3 is also a channel for H_2O_2, a molecule which can modulate intracellular signaling pathways[21]. To test whether the requirement for AQP3 in T cell activation was due to its ability to facilitate diffusion of H_2O_2 across membranes, we investigated if H_2O_2 is required for TCR/CD28-induced p-ERK. Initially we determined that 20 u/ml of catalase was sufficient to eliminate exogenously added 1 mM H_2O_2 (Supplementary Figure 7A). Subsequently, we showed that 20 u/ml catalase did not affect the TCR/CD28-induced p-ERK after 1 hour of stimulation, and the same was seen at 2 and 200 u/ml (Supplementary Figure 7B). Thus, we find no evidence that H_2O_2 is required for TCR-induced signaling to ERK activation. AQP3 can also transport glycerol[19]. However, this function is unlikely to account for the defect in TCR/CD28-induced p-ERK and proliferation in T cells treated with AQP3i in vitro, since there is no glycerol in the medium. Taken together, these results support our hypothesis that TCR signaling through WNK1, OXSR1 and STK39 results in AQP3-dependent water entry which is required for early TCR signaling as well as proliferation.

WNK1-dependent water influx is required for TCR signaling and G1 entry

To directly test whether TCR/CD28 signaling through WNK1 leads to water entry that is required for T cell activation, we stimulated WNK1-deficient $CD4^+$ T cells in hypotonic

medium, to force water entry by osmosis. Remarkably, we found that hypotonic medium restored much of the reduced TCR/CD28-stimulated p-ERK in WNK1^{D368A}-expressing T cells, and all of the reduced p-ERK in WNKi-treated T cells as measured 1 h after stimulation (Figure 7A-B, Supplementary Figure 8A-B). Furthermore, hypotonic medium also rescued the defect in TCR/CD28-induced Ki67 upregulation at 2 d (Figure 7C, Supplementary Figure 8C). The effect of hypotonic medium could be due to increased water entry into the cell but could also be caused by the reduced concentration of Na^+ and Cl^- ions in the medium. To distinguish these possibilities, we stimulated the T cells in isotonic medium that had the same reduced concentrations of Na^+ and Cl^- but the osmolarity was made isotonic with L-glucose, an inert osmolyte. Importantly, this isotonic medium with reduced Na^+ and Cl^- concentrations was unable to rescue the TCR/CD28-stimulated p-ERK at 1 h or the induction of Ki67 at 2 d in WNK1^{D368A}-expressing or WNKi-inhibited $CD4^+$ T cells (Figure 7A-C, Supplementary Figure 8A-C). Thus, the rescue seen with hypotonic medium was due to water entry, not reduced ion concentrations. Taken together, these results demonstrate that TCR/CD28 co-stimulation of $CD4^+$ T cells leads to water entry mediated by the WNK1-OXSR1-STK39-AQP3 signaling pathway, and this is required for TCR/CD28-induced ERK activation and entry into G1 (Figure 7D).

DISCUSSION

We show that WNK1 signaling through OXSR1, STK39 and AQP3 plays a central role in $CD4^+$ T cell proliferation in response to antigen, and thus the generation of a class-switched antibody response. WNK1 pathway activity is required for entry of naive $CD4^+$ T cells into G1 and progression through S and G2/M. More specifically, WNK1-dependent water influx, a previously unexplored component of the TCR signaling cascade, is required for TCR-induced ERK signaling and entry into G1. These two WNK1-dependent, water-

sensitive processes are probably linked as progression from G0 to G1 is strongly dependent on ERK activation[22].

Abrogation of WNK1 activity causes larger defects in TCR-induced p-ERK activation and proliferation than mutations in *Oxsr1* and *Stk39* or inhibition of AQP3, suggesting that WNK1 may in part function through other pathways to regulate cell proliferation. This may be due to redundancy, with signaling proteins functioning in parallel with OXSR1 and STK39, or with other AQP-family members. Nonetheless, we note that hypotonic medium rescues the defective TCR-induced p-ERK activation at 1 hour of stimulation and Ki67 induction after 2 days in WNKi-treated T cells. This strongly supports our proposal that TCR signaling through WNK1 results in water entry that is required for early TCR signaling and the transition from G0 to G1.

We hypothesize that TCR/CD28 signaling via WNK1 and OXSR1 and STK39 leads to SLC12A-dependent ion influx, which in turn drives water entry by osmosis through AQP3. We showed that TCR/CD28-induced ERK activation requires Na^+ and Cl^- ions and that WNK1 is required for SLC12A2 phosphorylation during $CD4^+$ T cell activation, but we were not able to demonstrate a functional requirement for SLC12A2, SLC12A6 or SLC12A7 in this process using inhibition and/or genetic deletion. This could be because we did not mutate or inhibit the key SLC12A-family members of the 5 expressed in $CD4^+$ T cells, or because other WNK1-regulated ion channels are more important. Beyond the SLC12A-family, WNK kinases have been reported to regulate several other channels including ENaC, CLC3 and TRP6[23]. Further work will be required to address these possibilities.

In the absence of WNK1 activity, T cells are smaller, and the TCR-induced volume increase is reduced compared to control cells. The volume decrease in WNKi-treated cells,

even in the absence of TCR stimulation, demonstrates a homeostatic role for WNK1 in controlling T cell volume. Indeed, WNK kinases are important for the regulatory volume increase that follows cell shrinkage induced by hypertonic conditions[4,9]. In the hypotonic rescue experiments, we propose that the resulting water entry would compensate for the defective regulatory volume increase in WNKi-inhibited T cells, as well as the defect in the additional WNK1-dependent TCR-induced volume increase.

Water entry alters several biophysical properties of the cell which could affect TCR signaling. Water influx increases membrane tension which has been shown to regulate signaling pathways[24-28]. Water entry also reduces molecular crowding, thereby increasing rates of intracellular signaling pathways[29], and decreases the viscosity of the cytoplasm, resulting in more rapid assembly of macromolecular structures such as microtubules[30]. Any or all of these changes could facilitate the assembly of the macromolecular TCR signaling complexes at the immune synapse and subsequent signal transduction[31]. Similarly, water entry could be required to facilitate the function of the macromolecular replisome complex, thereby accounting for the decreased rate of DNA replication in WNK1-deficient T cells. Furthermore, entry of water into T cells is presumably required to compensate for the rapid synthesis of macromolecules that accompanies T cell activation and entry into G1[32].

We also show that in the absence of WNK1-OXSR1-STK39-AQP3 signaling, ATR is activated and induces cell cycle arrest in G2. After 24 h, T cell division is no longer dependent on TCR signaling[33]. Thus, the requirement for water influx for T cells to progress through an ATR-dependent G2 checkpoint 72 h after the start of T cell activation is likely to be independent of TCR signaling. This TCR-independent function of the WNK1

pathway may reflect a homeostatic role in the regulation of cellular water content and volume or a specific role at the G2/M transition.

We found that inhibition of WNK1 resulted, unusually, in ATR activation independently of DNA damage. ATR is activated by mechanical stress at the nuclear envelope caused by a change in cell volume[34]. A similar mechanism may account for ATR activation in T cells in which the WNK1 pathway is inhibited, since this results in cell shrinkage. Interestingly, other studies have shown that compromised osmoregulation causes G2 arrest in multiple cell types, including T cells[35,36]. Thus, we have uncovered an ATR-dependent mechanism for a potentially universal osmotically-sensitive cell cycle checkpoint at G2/M, a possibility that warrants further study.

WNK1 may additionally regulate T cell proliferation by other mechanisms. In HeLa cells, WNK1 was shown to regulate the formation of mitotic spindles[37]. Furthermore, WNK1 is a negative regulator of autophagy in U2OS and HeLa cells, a cellular process that inhibits proliferation[38-40]. Finally, WNK1 regulates protein trafficking, so it may transduce signals by altering surface expression of AQP3 or other proteins required for proliferation[41-43]. These are interesting areas for future investigation.

Several observations suggest that WNK1-dependent water influx may be a common feature of mitogenic pathways in many cell types, both within the immune system and beyond. Firstly, WNK1 is broadly expressed[44]. Secondly, water influx occurs during mammalian cell division[45-47], and, thirdly, aquaporins are required for cell proliferation in several cell types[48-51]. Furthermore, we have recently found that WNK1 is activated in B cells by stimulation through the B cell antigen receptor and CD40, and that WNK1, OXSR1 and STK39 are required for proliferation induced by signals from both receptors[52]. Taken

together with our results, we propose that WNK1 pathway-driven water influx may be essential for the proliferation of multiple cell types.

More broadly, in a parallel study we have shown that chemokine receptor signaling in $CD4^+$ T cells activates the WNK1 pathway, leading to ion and water influx and that water entry is required for T cell migration[18]. This shows that activation of WNK1 and downstream ion and water influx is an important feature of signaling from several receptors and that it plays a role in both cell migration and proliferation and potentially in other physiological processes.

In summary, we have shown that TCR signaling via WNK1, OXSR1, STK39 and AQP3 leads to water influx, which is required for TCR signaling, T cell proliferation, and hence for T-dependent antibody responses.

MATERIALS AND METHODS

Mice

Mice with a conditional allele of *Wnk1* containing loxP sites flanking exon 2 (*Wnk1*^{tm1Clhu},*Wnk1*^{fl})[12], with a deletion of exon 2 of *Wnk1* (*Wnk1*$^{tm1.1Clhu}$, *Wnk1*$^{-}$), with a kinase-inactive allele of *Wnk1* (*Wnk1*$^{tm1.1Tyb}$, *Wnk1*^{D368A})[10], with a conditional allele of *Oxsr1* containing loxP sites flanking exons 9 and 10 (*Oxsr1*$^{tm1.1Ssy}$, *Oxsr1*^{fl})[53], with a tamoxifen-inducible Cre in the ROSA26 locus (*Gt(ROSA)26Sor*$^{tm1(Cre/ESR1)Thl}$, *ROSA26*^{CreERT2}, RCE)[13], with an allele of *Stk39* encoding STK39-T243A (*Stk39*$^{tm1.1Arte}$, *Stk39*^{T243A})[16] that cannot be activated by WNK1, deficient for RAG1 (*Rag1*^{tm1Mom}, *Rag1*$^{-}$)[54] or SLC12A2 (*Slc12a2*^{tm1Ges}, *Slc12a*$^{-}$)[55] or TCRα (*Tcra*^{tm1Mjo}, *Tcrα*$^{-}$)[56], expressing a tdTomato protein from the ROSA26 locus (*Gt(ROSA)26Sor*$^{tm4(ACTB-tdTomato-EGFP)Luo}$, *ROSA26*-mTmG)[57] and with transgenes encoding TCRα and TCRβ chains specific for chicken ovalbumin residues 323-339 (Tg($^{TcraTcrb)425Cbn}$, OT-II)[14] have been described before. C57BL/6J and B6SJLF1 mice were provided by the Biological Research Facility of the Francis Crick Institute. All genetically modified mice were maintained on a C57BL/6J background, housed in specific pathogen-free conditions, and given food and water *ad libitum*. All experiments were approved by the Francis Crick Institute Animal Welfare Ethical Review Board and were carried out under the authority of a Project Licence granted by the UK Home Office.

Bone marrow chimeras

RAG1-deficient recipient mice were irradiated with 1 dose of 5 Gy from a ^{37}Cs source. Bone marrow cells from *Wnk1*$^{fl/+}$RCE, *Wnk1*$^{fl/fl}$RCE, *Wnk1*$^{fl/D368A}$RCE, *Wnk1*$^{fl/+}$RCE OT-II, *Wnk1*$^{fl/fl}$RCE OT-II, *Oxsr1*$^{+/+}$*Stk39*$^{+/+}$RCE, *Oxsr1*$^{fl/fl}$*Stk39*$^{T243A/T243A}$RCE or *Tcrα*$^{-/-}$ mice or fetal livers from *Slc12a2*$^{+/+}$ or *Slc12a2*$^{-/-}$ E14.5 embryos were transferred intravenously into irradiated recipient mice which were maintained on 0.02% enrofloxacin (Baytril, Bayer

Healthcare) for 4 weeks. Both male and female mice were used, but in all cases the sex of the donor and recipient mice was matched. The hematopoietic compartment was allowed to reconstitute for at least 8 weeks after bone marrow transfer. In all experiments, control and experimental chimeric mice or cells derived from them were always age- and sex-matched.

In vivo deletion of floxed alleles

Mice were injected intraperitoneally with 2 mg tamoxifen (Sigma-Aldrich) in 100μL of corn oil (Sigma-Aldrich) on 3 (*Wnk1*^{fl}) or 5 (*Oxsr1*^{fl}) consecutive days. Mice were sacrificed 7 (*Wnk1*^{fl}) or 21 (*Oxsr1*^{fl}) days after initial tamoxifen injection.

NP-CGG immunization and ELISA

Mice were injected intraperitoneally with 50μg of 4-hydroxy-3-nitrophenylacetyl (NP)-CGG (BioSearch Technologies) in PBS, 25% Alum (Thermo Fisher Scientific). Blood was collected from the lateral tail vein at the indicated time points, allowed to clot, then centrifuged at 17,000 x *g* for 10 min. NP_{20}-BSA (bovine serum albumin) (5μg/ml, Santa Cruz Biotechnology) was used to coat 96-well Maxisorp Immunoplates (Nalge Nunc International Corporation) overnight at 4°C. Plates were washed with PBS, 0.01% Tween-20 (PBS-T), blocked with 3% BSA in PBS, and washed with PBS, 0.01% Tween-20. Serial dilutions of sera were incubated on the NP_{20}-BSA-coated plates overnight at 4°C. Plates were washed 3 times with PBS-T and incubated with 1.6 μg/ml biotin-conjugated goat anti-mouse IgM (Thermo Fisher Scientific) or 4 μg/ml biotin-conjugated goat anti-mouse IgG1 (Thermo Fisher Scientific) for 2 h at room temperature. Plates were washed with PBS-T 3 times, incubated with 1 μg/ml peroxidase-labelled streptavidin (Vector laboratories) for 2 h at room temperature, washed 5 times with PBS-T and incubated with 1x TMB ELISA

substrate solution (Thermo Fisher Scientific). The reaction was stopped with 2 N H_2SO_4. Absorption at 450 nm was measured using the SpectraMax 190 (Molecular Devices LLC.). Serum concentrations of NP-specific IgG and IgM antibodies were calculated in arbitrary units (a.u.) from the linear section of the response curves.

Cell isolation

Blood was harvested from live mice by cutting the lateral tail vein. Peripheral lymph nodes, mesenteric lymph nodes and spleens were dissociated into single cell suspensions by mashing through a 70 μm filter. Bone marrow from the hind limbs was harvested by flushing femurs and tibias with media. Blood, bone marrow, and spleen samples were treated with ACK buffer (155 mM NH_4Cl, 10 mM $KHCO_3$, 0.1 mM Na_2EDTA) for 3 min at room temperature to remove erythrocytes, washed and resuspended in PBS. ACK treatment was repeated twice for blood samples. To isolate naive $CD4^+$ T cells, lymph node cells were resuspended in a mixture of biotinylated antibodies against CD8, CD11b, CD11c, B220, CD19, CD25, CD44, and GR-1 (Table S1) in IMDM (35.93 mM NaCl, 0.18 mM Penicillin, 0.17 mM Streptomycin, IMDM powder, pH 7.2 [Thermo Fisher Scientific]), 5% fetal calf serum (FCS) for 20 min at 4°C. Cells were incubated with streptavidin-coated Dynabeads (Thermo Fisher Scientific) in IMDM, 5% FCS for 20 min at 4°C. Cell and bead suspensions were placed on a magnet for 2 min at room temperature and the bead-depleted fraction was collected.

CTV labelling of $CD4^+$ T cells

Naïve CD4+ T cells were incubated in PBS with CellTrace Violet (CTV, ThermoFisher) at a concentration of 5 μM (for OT-II T cells) or 2.5 μM (for polyclonal T cells) for 10 min at 37°C. A 5-fold excess of pre-warmed RPMI+ medium (RPMI-1640, 100 μM non-essential

amino acids, 20 mM HEPES [Thermo Fisher Scientific], 10% FCS, 100 U/mL Penicillin, 100 μg/mL Streptomycin, 2 mM L-glutamine, 100 μM 2-mercaptoethanol [Sigma-Aldrich]) was added to the cells for a further 7 min. Cells were then pelleted and resuspended in the appropriate media.

RNA isolation and quantitative reverse transcription- quantitative polymerase chain reaction (RT-qPCR)

RNA was purified from at least 5 x 10^4 $CD4^+$ T cells using the RNeasy Micro kit (Qiagen). cDNA was synthesized using the SuperScript™VILO™cDNA synthesis kit (Invitrogen). Taqman™ Gene Expression Assays (Thermo Fisher Scientific) were used to measure *Wnk1* (exon boundary 1-2, Mm01184006_m1), and *Hprt* (exon boundary 2-3, Mm03024075_m1). Fluorescence was measured using a QuantStudio 3 or QuantStudio 5 qPCR machine (Thermo Fisher Scientific).

Adoptive transfer of OT-II $CD4^+$ T cells

OT-II T cells ($CD45.1^-CD45.2^+$) were isolated from peripheral and mesenteric lymph nodes, labeled with CTV and 1 x 10^6 (for day 3 analysis) or 35 x 10^3 (for day 7 analysis) OT-II T cells were injected into the tail vein of B6SJLF1 mice ($CD45.1^+CD45.2^+$). 24 h later (day 0) mice were immunized with 50 μg (day 3 analysis) or 100 μg (day 7 analysis) chicken ovalbumin (OVA) protein (InvivoGen) in PBS, 25% Alum (Thermo Fisher Scientific) by intraperitoneal injection. Peripheral and mesenteric lymph nodes were harvested at day 3. Mesenteric lymph nodes, spleen and blood were harvested at day 7.

Co-culture of OT-II T cells with APCs

To generate APCs, bone marrow from C57BL/6J mice was treated with ACK and cultured

in DC medium (RPMI-1640 [Thermo Fisher Scientific], 10% FCS, 100 U/mL Penicillin, 100 μg/mL Streptomycin, 2 mM L-glutamine [Sigma-Aldrich]) with GM-CSF (20 ng/ml, Peprotech) at 10^6 cells/ml for 10 d at 37°C. GM-CSF was replenished at days 3, 5 and 7. Naïve $CD4^+$ OT-II T cells and APCs (both at 2.5 x 10^5 cells/ml) were co-cultured in round-bottomed 96-well plates in DC medium (RPMI-1640, 10% FCS, 100 U/mL Penicillin, 100 μg/mL Streptomycin, 2 mM L-glutamine [Sigma-Aldrich]) the presence of indicated concentrations of $OVA_{323-339}$ peptide (Sigma) for the indicated times.

Activation of T cells with plate-bound anti-CD3ε and anti-CD28 antibodies

Flat-bottomed multi-well cell culture plates (Corning) were incubated overnight at 4°C with PBS containing anti-CD3ε and anti-CD28 antibodies (4 μg/ml). Naïve $CD4^+$ T cells from peripheral and mesenteric lymph nodes were cultured at 1x10^6 cells/ml in RPMI+ at 37°C. Where indicated, cells were activated in the presence of 2.5 μM WNKi (WNK463, MedChem Express), 20 μM AQP3i (DFP00173, Axon MedChem), 20 μM SLC12A2i (bumetanide, Abcam) or 10 μM SLC12A6/7i (DIOA, Sigma) which were added from a stock solution in DMSO or the equivalent amount of DMSO as a vehicle only control. 1 μM ATRi (AZD6738, Selleckchem) or 4 mM hydroxyurea (HU, Sigma-Aldrich) were added for the final 36 h or 2 h of culture, respectively. For 1 h stimulations, naïve T cells were treated with 2.5 μM WNKi, 1μM MEKi (PD0325901, Selleckchem), 20 μM SLC12A2i, 10 μM SLC12A6/7i or vehicle only and transferred into anti-CD3ε/anti-CD28-coated multi-well plates, centrifuged at 340 x *g* for 30 s and incubated at 37°C for 1 h, still in the presence of inhibitors. To culture cells at different osmolarities, the concentration of NaCl in RPMI+ medium was adjusted and the osmolarity verified using an osmometer (Model 3250, Thermo Fisher Scientific). In some cases, isotonic (292 mOsm/l) RPMI+ medium was used in which some NaCl was replaced with L-glucose (G5500-5G, Sigma-Aldrich), an inert

osmolyte.

Activation of T cells with soluble anti-CD3ε and anti-CD28 antibodies

Naïve $CD4^+$ T cells were incubated in IMDM (Thermo Fisher Scientific), 0.5% FCS for 1 h at 37°C, cooled at 4°C for 10 min and then incubated with anti-CD3ε and anti-CD28 antibodies (10 μg/ml) in RPMI, 0.5% FCS in the presence of 2.5 μM WNKi, 100 nM SRCi (Dasatinib, Sigma-Aldrich) or vehicle only at 4°C for 30 min. Unstimulated (0 min) samples were incubated in the presence of relevant inhibitors but without anti-CD3ε or anti-CD28 antibodies. Cells were warmed to 37°C for 15 min and then stimulated with the addition of 80 μg/mL anti-Armenian hamster IgG (Antibodies-online.com). Activation was stopped at the indicated time point with the addition of 2% paraformaldehyde (PFA).

NaCl reduction and Cl replacement

To generate media of varying NaCl compositions, NaCl-free RPMI (Honeywell, S9888) was supplemented with additional NaCl. To make the medium isotonic, the remaining difference in osmolarity (up to 300 mOsm/L) was made up using L-glucose, an inert osmolyte. Osmolarity was verified using an osmometer (Model 3250, Advanced Instruments). To generate medium with reduced Cl concentration, NaCl-free RPMI was made isotonic through the addition of Na gluconate (Sigma, S2054-100G).

Cell volume measurement

Naïve $CD4^+$ T cells were rested overnight in RPMI+ with 1 mM pyruvate. Samples were enriched for live cells by incubating in PBS at 37°C for 10 min followed by 7 min at 37°C in RPMI+ with 1 mM pyruvate. Cells were then treated with vehicle only or 2.5 μM WNKi and placed in cell culture plates ± plate-bound anti-CD3ε and anti-CD28 for 1 h at 37°C.

Cell volume was measured using the CASY® cell counter (OMNI Life Science).

Alternatively, cell volume was determined using microscopy. Naïve CD4 T cells purified from ROSA-mTmG mice expressing tdTomato-CAAX to visualize the plasma membrane were placed in glass 8-well μ-slides (ibidi, 80827) coated with either anti-CD3ε and anti-CD28 antibodies (4 μg/ml) or poly-D-lysine (50 μg/mL, Sigma, A-003-M) and incubated at 37°C for 1 h. Cells were imaged using instant structural illumination microscopy (iSIM) using an iSIM microscope (VisiTech) with an Olympus 150x TIRF apo (1.45 NA) oil-immersion objective. Cells were excited using 552 nm wavelength laser, with emission detected using an sCMOS camera (Prime BSI Express, Teledyne Photometrics). Resulting images were deconvoluted using Microvolution algorithms in μ-Manager. Cell volume was calculated by generating a mask of plasma membrane edges and summing up the areas of individual z-slices in each cell measured using the 'analyze particles' function in FIJI.

Flow cytometry

Proliferation analysis

Cells were stained in PBS containing fluorophore-conjugated antibodies (Table S1) and LIVE/DEAD™ Near-IR dye (Thermo Fisher Scientific) (1:500) at 4°C for 20 min, and resuspended in FACS buffer (PBS, 0.5% BSA). For cell counting, a known number of Calibrate APC beads (BD biosciences) were added to the sample. Samples were analyzed on an LSRFortessa™ (BD biosciences) flow cytometer. Flow cytometry data were analyzed using FlowJo 9 and 10 (BD Biosciences).

CXCR5

Cells were incubated in PBS, 2% FCS containing biotinylated anti-CXCR5 antibody at 37°C for 30 min. Cells were washed, incubated with fluorophore-conjugated streptavidin for 15 min at room temperature, washed, resuspended in FACS buffer, and analyzed on the flow cytometer.

Analysis of phosphorylated proteins

Cells were fixed in 2% PFA at 4°C for 15 min, permeabilized with 90% methanol overnight at -20°C, washed 3 times and then incubated with the relevant primary antibody (Table S1) in PBS, 2% FCS for 30 min at room temperature. Cells were then washed, stained with the relevant secondary antibody in PBS, 2% FCS for 30 min at room temperature, washed, resuspended in FACS buffer, and analyzed on the flow cytometer.

Cell cycle analysis

To analyze the rate of S phase progression, 10 μM EdU (5-ethynyl-2'-deoxyuridine, Jena Bioscience) was added to the cell culture medium for 10 min at the end of 72 h culture on anti-CD3ε- and anti-CD28-coated cell culture plates. Cells were fixed in 4% PFA, permeabilized in BD Perm/Wash™ buffer (BD biosciences), 1% BSA at room temperature for 15 min. The Click reaction was initiated by adding 2 mM $CuSO_4$, 0.3125 μM AF488-azide, 10 mM Sodium Ascorbate (all from Jena Bioscience) in TBS (50 mM Tris, 150 mM NaCl, pH 7.5) for 30 min at room temperature. To analyze distribution of cells in different phases of the cell cycle, cells were stained with Live/Dead-Near IR stain (ThermoFisher Scientific) and fixed in 4% PFA for 15 min at 4°C, stained with fluorophore-conjugated antibodies against Ki67, p-MPM2 (Table S1) in BD Perm/Wash™ buffer (BD biosciences) containing 2% FCS for 30 min at room temperature, resuspended in BD Perm/Wash™ buffer containing 1 μg/mL FxCycle™ Violet (Thermo Fisher Scientific) to stain for DNA

content, incubated at room temperature for 30 min, and analyzed on the flow cytometer. In some experiments, cells were pulsed with EdU and analyzed as above. Ki67 was used to identify cells that had exited G0. The proportion of cells in G1, S, and G2/M was estimated using the Watson model generated from the histogram of DNA content of $Ki67^+$ cells. Staining for p-MPM2 was used to identify cells in M phase. Where indicated, cells were pulsed for 30 min with EdU at the end of 72 h culture and G2/M cells were identified as the 4n EdU^- population. The effect of expansion was taken out of the data by dividing the total number of $Ki67^+$ cells by the expansion index - the fold expansion of the population due to proliferation estimated by generating a model using CTV dilution histograms – to give $Ki67^+_{adjust}$. The percentage of $Ki67^+$ cells in the population if no division had taken place was then calculated as follows: $(Ki67^+_{adjust})/(Ki67^+_{adjust} + Ki67^-) \times 100\%$.

Immunoblot analysis

Cell pellets were thawed at room temperature, lysed using RIPA buffer (50 mM Tris, 150 mM NaCl, 50 mM NaF, 2 mM EDTA, 2 mM $Na_4P_2O_7$, 1 mM Na_3VO4, 1% Triton X-100, 0.5% deoxycholate, 0.1% SDS, 1 mM PMSF, cOmplete™ EDTA-free protease inhibitor cocktail [Roche], PhosSTOP™ [Roche]), centrifuged at 17,000 x *g* for 15 min at 4°C and the supernatant was collected. The protein concentration of each sample was determined using the Pierce™ BCA protein assay kit (Thermo Fisher Scientific) according to the manufacturer's instructions. Samples were mixed with NuPage™ LDS sample buffer (Thermo Fisher Scientific), 50 mM DTT and loaded onto NuPAGE™ 4-12% Bis-Tris precast polyacrylamide gels (Thermo Fisher Scientific) with the volume of each sample adjusted to ensure equal protein amounts per well. Electrophoresis was carried out at 200 V for 53 min in NuPAGE™ MOPS or MES SDS running buffer (Thermo Fisher Scientific). Proteins were transferred to a methanol-activated polyvinylidene difluoride membrane in NuPAGE™ transfer buffer (Thermo Fisher Scientific) at 30 V for 65 min. Membranes were

blocked with Odyssey® blocking buffer (LI-COR) for 1 h at room temperature, incubated with primary antibody (Table S1) in Odyssey® blocking buffer overnight at 4 °C, washed 3 times with TBS-T (TBS, 0.05% Tween20), incubated with fluorophore-conjugated secondary antibody (Table S1) in Odyssey® blocking buffer for 1 h at room temperature, washed 3 times with TBS-T, and imaged using the Odyssey® CLx (LI-COR). Image Studio Lite (LI-COR) was used to quantify intensities of bands.

RNA sequencing (RNAseq)

Wnk1$^{+/-}$RCE and *Wnk1*$^{-/-}$RCE CD4^{+} T cells were purified from lymph nodes of bone marrow radiation chimeras that had been treated with tamoxifen as described above. Cells were lysed using QIAzol lysis kit (Qiagen) and RNA was extracted using RNAeasy mini kit (Qiagen) according to the manufacturer's instructions. cDNA library synthesis was carried out using KAPA mRNA HyperPrep Kit (Illumina) and libraries were sequenced on the Illumina HiSeq 4000, acquiring 75 base single end reads. Reads were trimmed and adaptors removed using Trimmomatic (v 0.36). Reads were aligned with STAR (v 2.5.2a) using mouse genome assembly GRCm38, gene counts quantified with RSEM (v 1.2.31) and differential expression analysis was carried out with DESeq2[58]. Data has been deposited with GEO (accession number GSE201228, token for reviewer access: sjwfiomehtwvbgp).

Water permeability

Stopped-flow experiments were conducted at 25°C on a HiTech SF61 DX2 apparatus, equipped with a mercury−xenon lamp (TgK Scientific Ltd). Suspensions of naive CD4^{+} T cells (6x10^{6}/ml in PBS) were rapidly mixed with an equal volume of 300 mM mannitol in PBS to give an inwardly directed osmotic gradient of 150 mM. In the inhibitor experiments

2.5 μM WNK463 (WNKi) or 10 μM DFP00173 (AQP3i) were included in the solutions and were incubated for at least 15 min at room temperature before the measurements. Time courses of 90° light scattering were recorded at 450 nm with a 12 nm bandwidth over 60 s. At least four traces were measured for each biological replicate and averaged before data analysis. Scattering time traces were analysed in Kinetic Studio 5.0 (TgK Scientific Ltd) by fitting a single exponential curve to the data to determine the observed rate constant. Data from each batch of T cells were then normalized to the average of the rate constant obtained in the absence of inhibitor (relative rates).

Catalase treatment to eliminate H_2O_2

To establish the concentration of catalase required to eliminate H_2O_2, mouse $CD4^+$ T cells were loaded with DCFDA (ab113851, Abcam) according to the manufacturer's protocol. Cells were pre-treated with 0, 2, 20, 200U/ml bovine liver catalase (C40, Sigma Aldrich) for 30 min. Cells were treated with 1 mM H_2O_2 for 30 min at room temperature, and DCFDA fluorescence was measured by flow cytometry (LSRFortessa X-20, BD Biosciences). To measure the effect of eliminating H_2O_2 on TCR/CD28-induced ERK activation, $CD4^+$ T cells were incubated with 0, 2, 20, 200U/ml of catalase at 37°C for 30 min before transferring to anti-CD3ε, anti-CD28 precoated plates and incubated for 1 h. Cells were fixed, permeabilized and stained for pERK as described earlier.

Statistical analysis

The non-parametric Mann-Whitney U-test was used to analyze the difference between groups using GraphPad Prism 8.

Supplementary Materials

Supplementary Table 1

Supplementary Figures 1 to 8

Data and materials availability

Mouse strains available on request. RNAseq data has been deposited with GEO (accession number GSE201228). Data that support the findings of this study are available from the corresponding author upon reasonable request.

References

1. Miller, M.J., Safrina, O., Parker, I. & Cahalan, M.D. Imaging the single cell dynamics of CD4+ T cell activation by dendritic cells in lymph nodes. *J Exp Med* **200**, 847-56 (2004).
2. Qi, H. T follicular helper cells in space-time. *Nat Rev Immunol* **16**, 612-25 (2016).
3. McCormick, J.A. & Ellison, D.H. The WNKs: atypical protein kinases with pleiotropic actions. *Physiol Rev* **91**, 177-219 (2011).
4. Shekarabi, M. *et al.* WNK Kinase Signaling in Ion Homeostasis and Human Disease. *Cell Metab* **25**, 285-299 (2017).
5. Alessi, D.R. *et al.* The WNK-SPAK/OSR1 pathway: master regulator of cation-chloride cotransporters. *Sci Signal* **7**, re3 (2014).
6. Thastrup, J.O. *et al.* SPAK/OSR1 regulate NKCC1 and WNK activity: analysis of WNK isoform interactions and activation by T-loop trans-autophosphorylation. *Biochem J* **441**, 325-37 (2012).
7. Vitari, A.C., Deak, M., Morrice, N.A. & Alessi, D.R. The WNK1 and WNK4 protein kinases that are mutated in Gordon's hypertension syndrome phosphorylate and activate SPAK and OSR1 protein kinases. *Biochem J* **391**, 17-24 (2005).
8. Vitari, A.C. *et al.* Functional interactions of the SPAK/OSR1 kinases with their upstream activator WNK1 and downstream substrate NKCC1. *Biochem J* **397**, 223-31 (2006).
9. de Los Heros, P., Pacheco-Alvarez, D. & Gamba, G. Role of WNK Kinases in the Modulation of Cell Volume. *Curr Top Membr* **81**, 207-235 (2018).
10. Köchl, R. *et al.* WNK1 kinase balances T cell adhesion versus migration in vivo. *Nat Immunol* **17**, 1075-83 (2016).
11. Köchl, R. *et al.* Critical role of WNK1 in MYC-dependent early mouse thymocyte development. *Elife* **9**, e56934 (2020).

12. Xie, J. *et al.* Endothelial-specific expression of WNK1 kinase is essential for angiogenesis and heart development in mice. *Am J Pathol* **175**, 1315-27 (2009).

13. de Luca, C. *et al.* Complete rescue of obesity, diabetes, and infertility in db/db mice by neuron-specific LEPR-B transgenes. *J Clin Invest* **115**, 3484-93 (2005).

14. Barnden, M.J., Allison, J., Heath, W.R. & Carbone, F.R. Defective TCR expression in transgenic mice constructed using cDNA-based alpha- and beta-chain genes under the control of heterologous regulatory elements. *Immunol Cell Biol* **76**, 34-40 (1998).

15. Yamada, K. *et al.* Small-molecule WNK inhibition regulates cardiovascular and renal function. *Nat Chem Biol* **12**, 896-898 (2016).

16. Rafiqi, F.H. *et al.* Role of the WNK-activated SPAK kinase in regulating blood pressure. *EMBO Mol Med* **2**, 63-75 (2010).

17. Roose, J.P., Mollenauer, M., Ho, M., Kurosaki, T. & Weiss, A. Unusual interplay of two types of Ras activators, RasGRP and SOS, establishes sensitive and robust Ras activation in lymphocytes. *Mol Cell Biol* **27**, 2732-45 (2007).

18. de Boer, L.L. *et al.* T cell migration requires ion and water influx to regulate actin polymerization. *bioRxiv*, 2022.03.16.484584 (2023).

19. Verkman, A.S. Aquaporins at a glance. *J Cell Sci* **124**, 2107-12 (2011).

20. Sonntag, Y. *et al.* Identification and characterization of potent and selective aquaporin-3 and aquaporin-7 inhibitors. *J Biol Chem* **294**, 7377-7387 (2019).

21. Miller, E.W., Dickinson, B.C. & Chang, C.J. Aquaporin-3 mediates hydrogen peroxide uptake to regulate downstream intracellular signaling. *Proc Natl Acad Sci U S A* **107**, 15681-6 (2010).

22. Appleman, L.J., van Puijenbroek, A.A., Shu, K.M., Nadler, L.M. & Boussiotis, V.A. CD28 costimulation mediates down-regulation of p27kip1 and cell cycle

progression by activation of the PI3K/PKB signaling pathway in primary human T cells. *J Immunol* **168**, 2729-36 (2002).

23. Xiu, M., Li, L., Li, Y. & Gao, Y. An update regarding the role of WNK kinases in cancer. *Cell Death Dis* **13**, 795 (2022).
24. Diz-Munoz, A. *et al.* Membrane Tension Acts Through PLD2 and mTORC2 to Limit Actin Network Assembly During Neutrophil Migration. *PLoS Biol* **14**, e1002474 (2016).
25. Katsumi, A. *et al.* Effects of cell tension on the small GTPase Rac. *J Cell Biol* **158**, 153-64 (2002).
26. Masters, T.A., Pontes, B., Viasnoff, V., Li, Y. & Gauthier, N.C. Plasma membrane tension orchestrates membrane trafficking, cytoskeletal remodeling, and biochemical signaling during phagocytosis. *Proc Natl Acad Sci U S A* **110**, 11875-80 (2013).
27. Houk, A.R. *et al.* Membrane tension maintains cell polarity by confining signals to the leading edge during neutrophil migration. *Cell* **148**, 175-88 (2012).
28. Rossy, J., Laufer, J.M. & Legler, D.F. Role of Mechanotransduction and Tension in T Cell Function. *Front Immunol* **9**, 2638 (2018).
29. Miermont, A. *et al.* Severe osmotic compression triggers a slowdown of intracellular signaling, which can be explained by molecular crowding. *Proc Natl Acad Sci U S A* **110**, 5725-30 (2013).
30. Molines, A.T. *et al.* Physical properties of the cytoplasm modulate the rates of microtubule polymerization and depolymerization. *Dev Cell* **57**, 466-479 (2022).
31. Campi, G., Varma, R. & Dustin, M.L. Actin and agonist MHC-peptide complex-dependent T cell receptor microclusters as scaffolds for signaling. *J Exp Med* **202**, 1031-6 (2005).

32. Wolf, T. *et al.* Dynamics in protein translation sustaining T cell preparedness. *Nat Immunol* **21**, 927-937 (2020).

33. Au-Yeung, B.B. *et al.* A sharp T-cell antigen receptor signaling threshold for T-cell proliferation. *Proc Natl Acad Sci U S A* **111**, E3679-88 (2014).

34. Kumar, A. *et al.* ATR mediates a checkpoint at the nuclear envelope in response to mechanical stress. *Cell* **158**, 633-646 (2014).

35. Drews-Elger, K., Ortells, M.C., Rao, A., Lopez-Rodriguez, C. & Aramburu, J. The transcription factor NFAT5 is required for cyclin expression and cell cycle progression in cells exposed to hypertonic stress. *PLoS One* **4**, e5245 (2009).

36. Kong, H. *et al.* AQP4 knockout impairs proliferation, migration and neuronal differentiation of adult neural stem cells. *J Cell Sci* **121**, 4029-36 (2008).

37. Tu, S.W., Bugde, A., Luby-Phelps, K. & Cobb, M.H. WNK1 is required for mitosis and abscission. *Proc Natl Acad Sci U S A* **108**, 1385-90 (2011).

38. Gallolu Kankanamalage, S. *et al.* WNK1 is an unexpected autophagy inhibitor. *Autophagy* **13**, 969-970 (2017).

39. Gallolu Kankanamalage, S. *et al.* Multistep regulation of autophagy by WNK1. *Proc Natl Acad Sci U S A* **113**, 14342-14347 (2016).

40. Wang, R.C. & Levine, B. Autophagy in cellular growth control. *FEBS Lett* **584**, 1417-26 (2010).

41. He, G., Wang, H.R., Huang, S.K. & Huang, C.L. Intersectin links WNK kinases to endocytosis of ROMK1. *J Clin Invest* **117**, 1078-87 (2007).

42. Oh, E., Heise, C.J., English, J.M., Cobb, M.H. & Thurmond, D.C. WNK1 is a novel regulator of Munc18c-syntaxin 4 complex formation in soluble NSF attachment protein receptor (SNARE)-mediated vesicle exocytosis. *J Biol Chem* **282**, 32613-22 (2007).

43. Lee, B.H. *et al.* WNK1 phosphorylates synaptotagmin 2 and modulates its membrane binding. *Mol Cell* **15**, 741-51 (2004).

44. Shekarabi, M. *et al.* Comparative analysis of the expression profile of Wnk1 and Wnk1/Hsn2 splice variants in developing and adult mouse tissues. *PLoS One* **8**, e57807 (2013).

45. Li, Y. *et al.* Going with the Flow: Water Flux and Cell Shape during Cytokinesis. *Biophys J* **113**, 2487-2495 (2017).

46. Saragovi, A. *et al.* Analysis of cellular water content in T cells reveals a switch from slow metabolic water gain to rapid water influx prior to cell division. *J Biol Chem* **298**, 101795 (2022).

47. Zlotek-Zlotkiewicz, E., Monnier, S., Cappello, G., Le Berre, M. & Piel, M. Optical volume and mass measurements show that mammalian cells swell during mitosis. *J Cell Biol* **211**, 765-74 (2015).

48. Serna, A. *et al.* Functional inhibition of aquaporin-3 with a gold-based compound induces blockage of cell proliferation. *J Cell Physiol* **229**, 1787-801 (2014).

49. Galan-Cobo, A., Ramirez-Lorca, R., Toledo-Aral, J.J. & Echevarria, M. Aquaporin-1 plays important role in proliferation by affecting cell cycle progression. *J Cell Physiol* **231**, 243-56 (2016).

50. Galan-Cobo, A., Ramirez-Lorca, R. & Echevarria, M. Role of aquaporins in cell proliferation: What else beyond water permeability? *Channels (Austin)* **10**, 185-201 (2016).

51. Hara-Chikuma, M. & Verkman, A.S. Aquaporin-3 facilitates epidermal cell migration and proliferation during wound healing. *J Mol Med (Berl)* **86**, 221-31 (2008).

52. Hayward, D.A. *et al.* B cell-intrinsic requirement for WNK1 kinase in antibody responses in mice. *J Exp Med* **220**, e20211827 (2023).

53. Lin, S.H. *et al.* Impaired phosphorylation of Na(+)-K(+)-2Cl(-) cotransporter by oxidative stress-responsive kinase-1 deficiency manifests hypotension and Bartter-like syndrome. *Proc Natl Acad Sci U S A* **108**, 17538-43 (2011).

54. Mombaerts, P. *et al.* RAG-1-deficient mice have no mature B and T lymphocytes. *Cell* **68**, 869-877 (1992).

55. Flagella, M. *et al.* Mice lacking the basolateral Na-K-2Cl cotransporter have impaired epithelial chloride secretion and are profoundly deaf. *J Biol Chem* **274**, 26946-55 (1999).

56. Philpott, K.L. *et al.* Lymphoid development in mice congenitally lacking T cell receptor alpha beta-expressing cells. *Science* **256**, 1448-52 (1992).

57. Muzumdar, M.D., Tasic, B., Miyamichi, K., Li, L. & Luo, L. A global double-fluorescent Cre reporter mouse. *Genesis* **45**, 593-605 (2007).

58. Love, M.I., Huber, W. & Anders, S. Moderated estimation of fold change and dispersion for RNA-seq data with DESeq2. *Genome Biol* **15**, 550 (2014).

Acknowledgments

We thank Erik Sahai and Simon Boulton for critical reading of the manuscript. We thank Matt Renshaw for help with image analysis and the Structural Biology Facility of the Francis Crick Institute for help with stopped flow. We thank Souradeep Basu, Subramanian Venkatesan, Daisy Luff, Darryl Hayward, Edina Schweighoffer, Simon Boulton, and Rob de Bruin for advice. We thank the Flow Cytometry, Advanced Light Microscopy and Biological Research Facilities of the Francis Crick Institute for flow cytometry, imaging and animal husbandry. We thank Chou-Long Huang, Dario Alessi and Sung-Sen Yang for mouse strains.

Funding

VLJT was supported by the Francis Crick Institute which receives its core funding from Cancer Research UK (CC2080), the UK Medical Research Council (CC2080), and the Wellcome Trust (CC2080), and by a grant from UKRI Biotechnology and Biological Sciences Research Council (BB/V0088757/1). LLdB was funded by an Imperial College London President's PhD Scholarship. For the purpose of Open Access, the author has applied a CC-BY public copyright licence to any Author Accepted Manuscript version arising from this submission.

Author Contributions

Conceptualization: JBOM, VLJT

Data curation: JBOM

Formal analysis: JBOM, LdB, ML

Funding acquisition: VLJT

Investigation: JBOM, LV, LdB, HH, DH, RK, SK, DL

Methodology: JBOM, RK

Project administration: VLJT

Resources: RK

Supervision: VLJT

Visualization: JBOM

Writing – original draft: JBOM, VLJT

Writing – review & editing: JBOM, VLJT

Competing interests

The authors have no competing interests.

Figure 1. WNK1 is essential for the generation of T_{FH} cells and class-switched antibody responses.

(**A-B**) Irradiated RAG1-deficient mice were reconstituted with a mixture of bone marrow from TCRα-deficient (TCRα$^{-/-}$) mice and either *Wnk1*$^{fl/+}$RCE or *Wnk1*$^{fl/-}$RCE mice, treated with tamoxifen at least 8 weeks later to delete *Wnk1*^{fl} alleles and immunized with NP-CGG in alum (A). NP-specific IgG1 antibodies in the serum quantified by ELISA at the time points indicated (B) (n = 10-18). Each point represents a different mouse, line indicates median. (**C-J**) Irradiated RAG1-deficient mice were reconstituted with bone marrow from *Wnk1*$^{fl/+}$RCE OT-II or *Wnk1*$^{fl/-}$RCE OT-II mice, treated with tamoxifen, and 7 d later naïve *Wnk1*$^{+/-}$ or *Wnk1*$^{-/-}$ CD4^{+} OT-II T cells (CD45.1^{-}CD45.2^{+}) were isolated, labelled with CTV, adoptively transferred into WT (CD45.1^{+}CD45.2^{+}) mice that were subsequently immunized with OVA in alum, and 3 or 7 days later, lymph node cells were analyzed by flow cytometry (C). CTV dilution at day 3 (D) was used to calculate the percentage of cells that had divided at least once (E, n = 7) and the proliferation index (average number of divisions by dividing cells) (F, n = 8). CD4^{+}CD45.1^{-}CD45.2^{+} OT-II T cells as a percentage of all CD4^{+} cells in peripheral and mesenteric lymph nodes at day 3 (G), and in the indicated tissues at day 7 (H, n=4). Splenic T_{FH} (PD-1^{hi}CXCR5^{+}) cell numbers (I) and percentage of all OT-II T cells day 7 (J, n=4). Each point represents a different mouse. Horizontal lines show median. Data are from 1 experiment representative of 2 (G) or 3 (H-J) experiments, or pooled from 2 independent experiments (B, E-F). a.u., arbitrary units. Statistical analysis with the Mann-Whitney U test. *0.01 < p < 0.05; **0.001 < p < 0.01; ***0.0001 < p < 0.001.

Figure 2. WNK1, OXSR1, and STK39 are required for TCR-induced proliferation of CD4^{+} T cells.

(**A-B**) WNK1-expressing or -deficient CTV-labelled OT-II CD4^{+} T cells were co-cultured with bone marrow-derived APCs in the presence of indicated concentrations of $OVA_{323-339}$

peptide for 5 days. CTV dilution (A) was used to determine the percentage of cells that had divided at day 3 (n = 5) (B). (**C-J**) Naïve $CD4^+$ CTV-labelled T cells of the indicated genotypes (C-F, I-J) or treated with WNKi (G-H) were activated on plate-bound anti-CD3ε and anti-CD28 antibodies for indicated times. CTV dilution (C, E, G, I) was used to determine the percentage of cells that had divided (n = 4-7) (D, F, H, J). WNKi, WNK inhibitor (WNK463). Each point represents a different mouse; horizontal lines show median; data are from 1 experiment representative of 2 (B, H) or 3 (D, J) experiments, or pooled from 2 independent experiments (F). Statistical analysis with the Mann-Whitney U test. *$0.01 < p < 0.05$; **$0.001 < p < 0.01$.

Figure 3. Loss of WNK1, or OXSR1 and STK39 impairs cell cycle progression of $CD4^+$ T cells.

(**A-J**) Naive $CD4^+$ T cells of the indicated genotypes, or treated with indicated inhibitors, were activated on plate-bound anti-CD3ε and anti-CD28 antibodies for 3 days. Graphs show percentage of $Ki67^+$ cells (after adjusting for population expansion) (A, F), and DNA content of $Ki67^+$ cells (B, G) which was used to estimate the median (± 95% CI) percentage of cells in different cell cycle phases at day 3 (C, H). Cells were pulsed with EdU for 10 min and incorporation of EdU (D, I) was used to calculate the rate of EdU incorporation (ΔEdU) by subtracting the average EdU MFI in G1 and G2/M phase cells from the average EdU MFI in S phase (n = 5-7) (E, J) using the gates shown. Each point represents a different mouse; horizontal lines or columns show median; data pooled from 2 independent experiments (A, C, F, H, J) or from 1 experiment representative of 2 (E) experiments. Statistical analysis with the Mann-Whitney U test. * $0.01 < p < 0.05$; ** $0.001 < p < 0.01$, **** $p < 0.0001$.

Figure 4. The WNK1 pathway regulates early TCR signaling and the ATR-mediated G2/M checkpoint.

(**A**-**C**) Naïve WT CD4$^+$ T cells were activated using soluble anti-CD3ε and anti-CD28 antibodies in the presence of indicated inhibitors and analyzed by flow cytometry. Graphs show median (± 95% CI) levels of p-CD3ζ (Y142) (A), p-ZAP70 (Y319) (B), and p-ERK1/2 (T202/Y204) (C) (n = 4); example histograms of flow data shown in Supplementary Figure 5A-C. (**D, E**) CD4$^+$ T cells of the indicated genotypes or in the presence of the indicated inhibitors were cultured for 1 h in the presence or absence of plate-bound anti-CD3ε and anti-CD28 antibodies. Graphs show the percentage of cells that were p-ERK high as determined by flow cytometry, gating as in Supplementary Figure 5D-E (n = 6-9). (**F-H**) CD4$^+$ T cells were cultured for 3 d on plate-bound anti-CD3ε and anti-CD28 antibodies, with ATRi or vehicle only added to cultures for the final 36 h. Graph of the abundance of p-CHK1 (S345) determined using immunoblots (example immunoblots below graph) (F, G) (n = 4-11). p-CHK1 was normalized to tubulin and to the mean signal in WNKi-treated cells (F) or *Oxsr1*$^{-/-}$*Stk39*$^{T243A/T243A}$RCE cells (G) which was set to 1. Graph showing percentage of CD4$^+$ cells in G2/M phase (EdU$^-$, 4n), gating as in Supplementary Figure 4E (n = 6) (H). WNKi, WNK inhibitor (WNK463); SRCi, SRC inhibitor (Dasatinib); AQP3i, AQP3 inhibitor (DFP00173); ATRi, ATR inhibitor (AZD6738). Each point represents a different mouse; columns show median. Data pooled from 2 (A-D, G, H) or 3 (E) independent experiments or from 1 experiment representative of 5 (F). Statistical analysis carried out using the Mann-Whitney U test. * $0.01 < p < 0.05$; ** $0.001 < p < 0.01$, *** $0.0001 < p < 0.001$, **** $p < 0.0001$.

Figure 5. Na and Cl are required for TCR-induced activation.

(**A, B**) $CD4^+$ T cells were cultured for 1 h in the presence or absence of plate-bound anti-CD3ε and anti-CD28 antibodies in medium in which different proportions of NaCl were replaced with L-glucose (A) or where the NaCl was replaced with Na gluconate (B), in both cases maintaining isotonicity. Note that the medium contains Na^+ and Cl^- from other constituents other than NaCl. Graphs show percentage p-ERK high cells (n=5-6). (**C**) mRNA levels of *Scl12a* genes in *Wnk1*$^{+/-}$ $CD4^+$ T cells determined by RNAseq; tpm, transcripts per million reads (n=6). (**D**) Levels of p-SLC12A2 in $CD4^+$ T cells cultured for 1 h in the presence or absence of plate-bound anti-CD3ε and anti-CD28 antibodies, with or without WNKi, measured by flow cytometry and normalized to the mean signal in stimulated cells without inhibitor (n=6). WNKi, WNK inhibitor (WNK463). Each point represents a different mouse; lines show median. Data is pooled from 2 experiments (A, B, D) or is from 1 experiment (C). Mann-Whitney U test; ** $0.001 < p < 0.01$, **** $p < 0.0001$.

Figure 6. WNK1-dependent volume changes and AQP3-dependent TCR-induced proliferation.

(**A**) Volume of naïve WT $CD4^+$ T cells activated for 1 h in the presence of vehicle only or WNKi on plate-bound anti-CD3ε and anti-CD28 antibodies where indicated, determined using a Casy® cell counter and normalized to the mean volume of cells in the absence of stimulation or inhibitor. Each dot represents the modal volume of ≥200 cells (n = 9). (**B**) Orthogonal sections of 3D images of mouse naïve $CD4^+$ T cells constitutively expressing tdTomato-CAAX, stimulated for 1 h on plate-bound anti-CD3ε and anti-CD28 antibodies with WNKi or vehicle only. Grey scale represents the tdTomato fluorescence intensity. White dashed lines show positions of the orthogonal slices which were taken at the widest and highest point of the cell. Blue dashed line represents the outline of the vehicle control

cell superimposed on the WNKi-treated cell. Green arrows show the location of the cell/slide interface in the XZ and YZ sections. Scale bars, 5 µm. (**C**) Cell volume measured by imaging of $CD4^+$ T cells stimulated for 1 h with plate-bound anti-CD3ε and anti-CD28 antibodies as indicated, with or without WNKi, representative images shown in B. Each dot represents 1 cell, violin plots show median and 25% and 75% quartiles (n=50-60). (**D**) mRNA levels of *Aqp* genes in *Wnk1*$^{+/-}$ $CD4^+$ T cells determined by RNAseq; tpm, transcripts per million reads (n=6). (**E**) Water permeability of $CD4^+$ T cells treated with or without AQP3i determined by measuring volume changes in response to an inwardly directed osmotic gradient of 150 mM mannitol. Graph shows relative rate constant normalized to the mean of cells with no inhibitor. Column shows mean, dots represent individual biological replicates. (**F, G**) Naïve $CD4^+$ CTV-labelled T cells treated with AQP3i were activated on plate-bound anti-CD3ε and anti-CD28 antibodies for indicated times. CTV dilution (F) was used to determine the percentage of cells that had divided (n = 4-5) (G). Data are pooled from 2 independent experiments (A, C, E), from 1 experiment representative of 2 (G) or from a single experiment (D). WNKi, WNK inhibitor (WNK463); AQP3i, AQP3 inhibitor (DFP00173). Statistical analysis with the Mann-Whitney test. * $0.01 < p < 0.05$; ** $0.001 < p < 0.01$. *** $0.0001 < p < 0.001$. **** $p < 0.0001$.

Figure 7. **WNK1-dependent water influx is required for TCR signaling and G1 entry.** (**A, B**) $CD4^+$ T cells of the indicated genotypes or in the presence of the indicated inhibitors were cultured for 1 h in the presence or absence of plate-bound anti-CD3ε and anti-CD28 antibodies. In some cultures, tonicities were altered by modulating concentrations of NaCl and L-glucose. Graphs show the percentage of cells that were p-ERK high as determined by flow cytometry, gating as in Supplementary Figure 8A-B (n = 5). (**C**) $CD4^+$ T cells were cultured on plate-bound anti-CD3ε and anti-CD28 antibodies for 2 days at the indicated

tonicities. Graph shows percentage of Ki67^{+} cells (after adjusting for population expansion) measured by flow cytometry, gating as in Supplementary Figure 8C (n = 10). (**D**) Proposed model of how TCR/CD28 signals via WNK1, OXSR1, STK39 and SLC12A-family ion co-transporters (SLC12A2 shown as an example) lead to ion influx and subsequent water entry through AQP3 by osmosis, which is required for TCR/CD28 signaling and T cell proliferation. We have not been able to directly demonstrate a role for SLC12A2, potentially because other SLC12A-family members are more important, acting alone or in combination or because other WNK1-regulated ion channels are involved. Water entry is required for early TCR signaling and for the transition from G0 to G1. In addition, the WNK1 pathway inhibits ATR and thereby allows cells to transit the G2/M checkpoint. WNKi, WNK inhibitor (WNK463). Each point represents a different mouse; columns show median. Data pooled from 2 (C) or from 1 experiment representative of >2 (A, B) experiments. Statistical analysis carried out using the Mann-Whitney U test. ns, not significant; * $0.01 < p < 0.05$; ** $0.001 < p < 0.01$; *** $0.0001 < p < 0.001$; **** $p < 0.0001$.

Figure 1

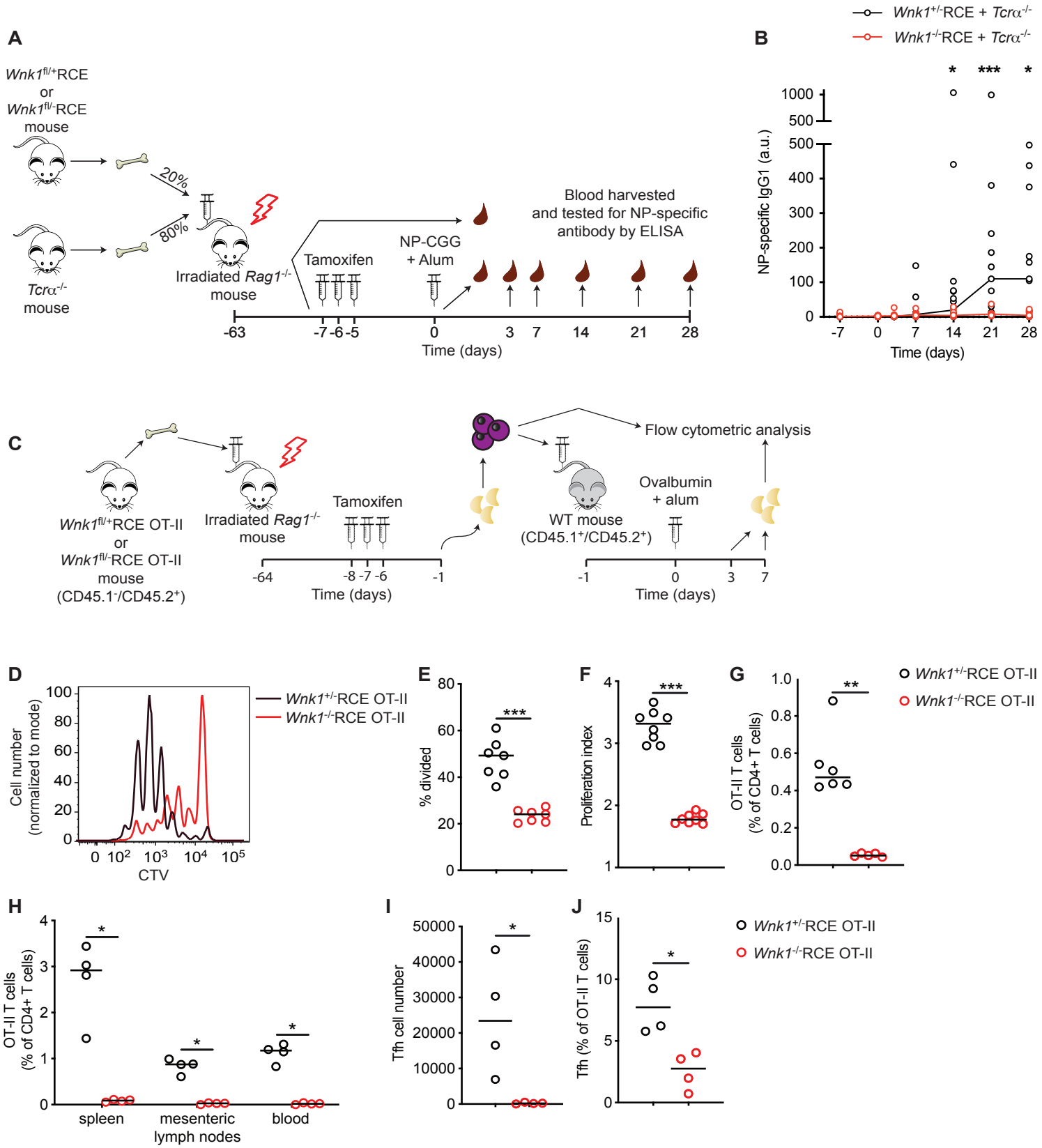
A
Wnk1fl/+RCE
or
Wnk1fl/-RCE
mouse
20%
80%
Tcrα-/-
mouse
Irradiated Rag1-/-
mouse
Tamoxifen
NP-CGG
+ Alum
Blood harvested
and tested for NP-specific
antibody by ELISA
-63
-7 -6 -5
0
3 7
14
21
28
Time (days)
B
Wnk1+/-RCE + Tcrα-/-
Wnk1-/-RCE + Tcrα-/-
NP-specific IgG1 (a.u.)
Time (days)
C
Wnk1fl/+RCE OT-II
or
Wnk1fl/-RCE OT-II
mouse
(CD45.1-/CD45.2+)
Irradiated Rag1-/-
mouse
Tamoxifen
-64
-8 -7 -6
-1
Time (days)
Flow cytometric analysis
WT mouse
(CD45.1+/CD45.2+)
Ovalbumin
+ alum
-1
0
3
7
Time (days)
D
Cell number
(normalized to mode)
CTV
Wnk1+/-RCE OT-II
Wnk1-/-RCE OT-II
E
% divided
F
Proliferation index
G
OT-II T cells
(% of CD4+ T cells)
H
OT-II T cells
(% of CD4+ T cells)
spleen
mesenteric
lymph nodes
blood
I
Tfh cell number
J
Tfh (% of OT-II T cells)

Figure 2

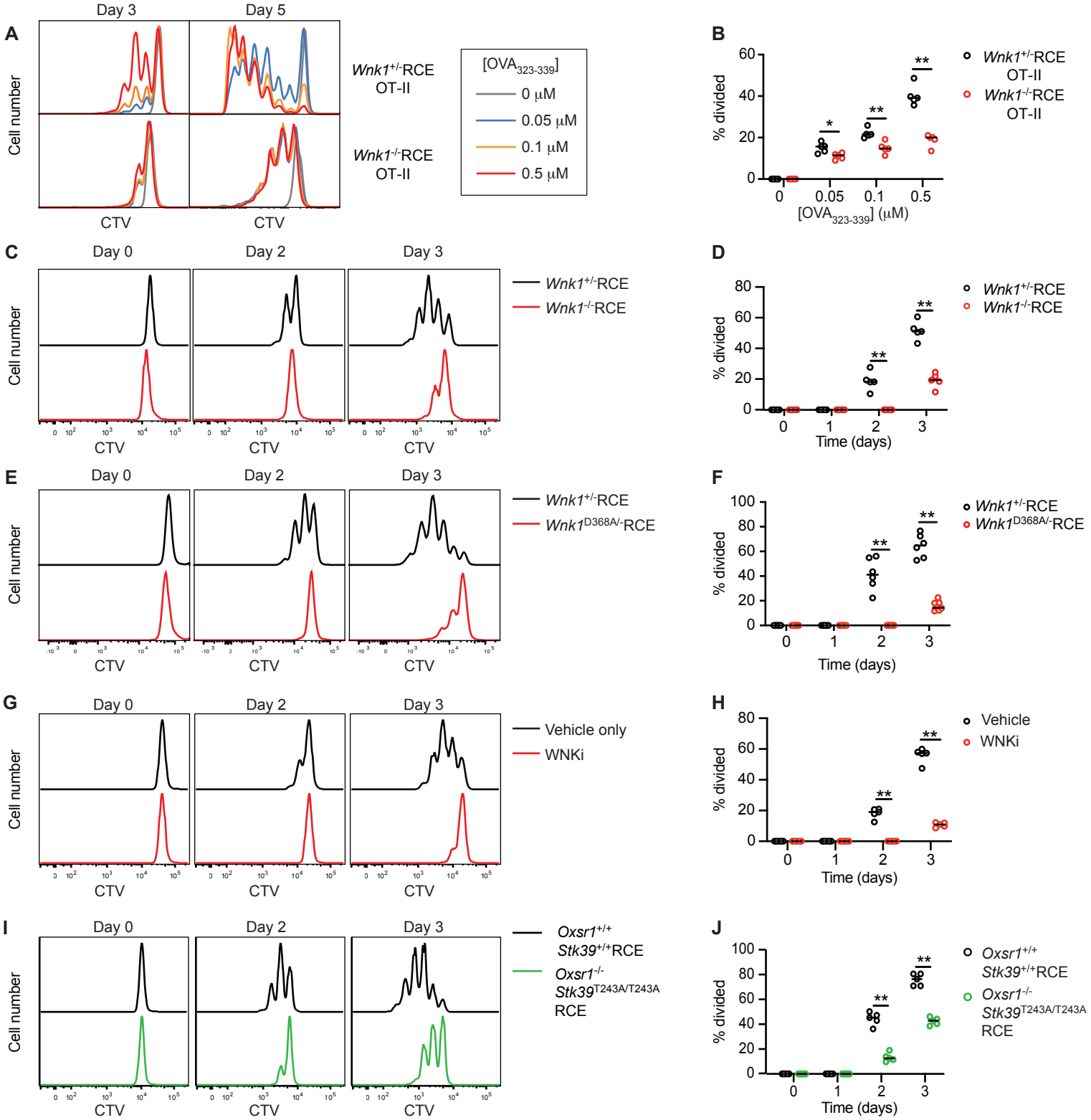
A
Day 3
Day 5
Cell number
CTV
Wnk1+/-RCE OT-II
Wnk1-/-RCE OT-II
[OVA323-339]
0 μM
0.05 μM
0.1 μM
0.5 μM
B
% divided
[OVA323-339] (μM)
Wnk1+/-RCE OT-II
Wnk1-/-RCE OT-II
C
Day 0
Day 2
Day 3
Wnk1+/-RCE
Wnk1-/-RCE
D
Time (days)
E
Wnk1D368A/-RCE
F
G
Vehicle only
WNKi
H
Vehicle
I
Oxsr1+/+ Stk39+/+RCE
Oxsr1-/- Stk39T243A/T243A RCE
J

Figure 3

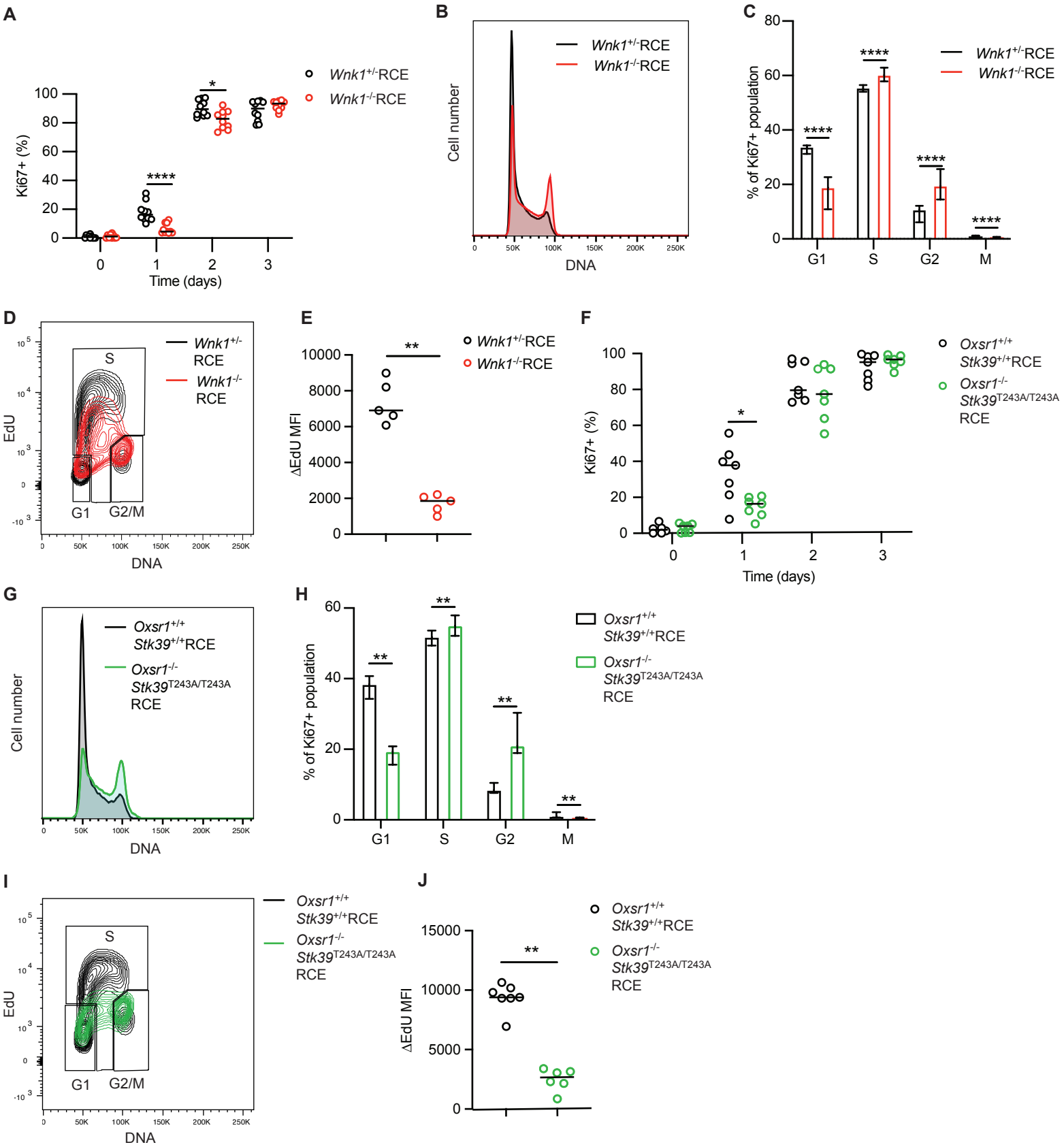
A
Ki67+ (%)
Time (days)
Wnk1+/-RCE
Wnk1-/-RCE
B
Cell number
DNA
C
% of Ki67+ population
G1
S
G2
M
D
EdU
DNA
G1
G2/M
S
E
ΔEdU MFI
F
Ki67+ (%)
Time (days)
Oxsr1+/+ Stk39+/+RCE
Oxsr1-/- Stk39T243A/T243A RCE
G
Cell number
DNA
H
% of Ki67+ population
I
EdU
DNA
J
ΔEdU MFI

Figure 4

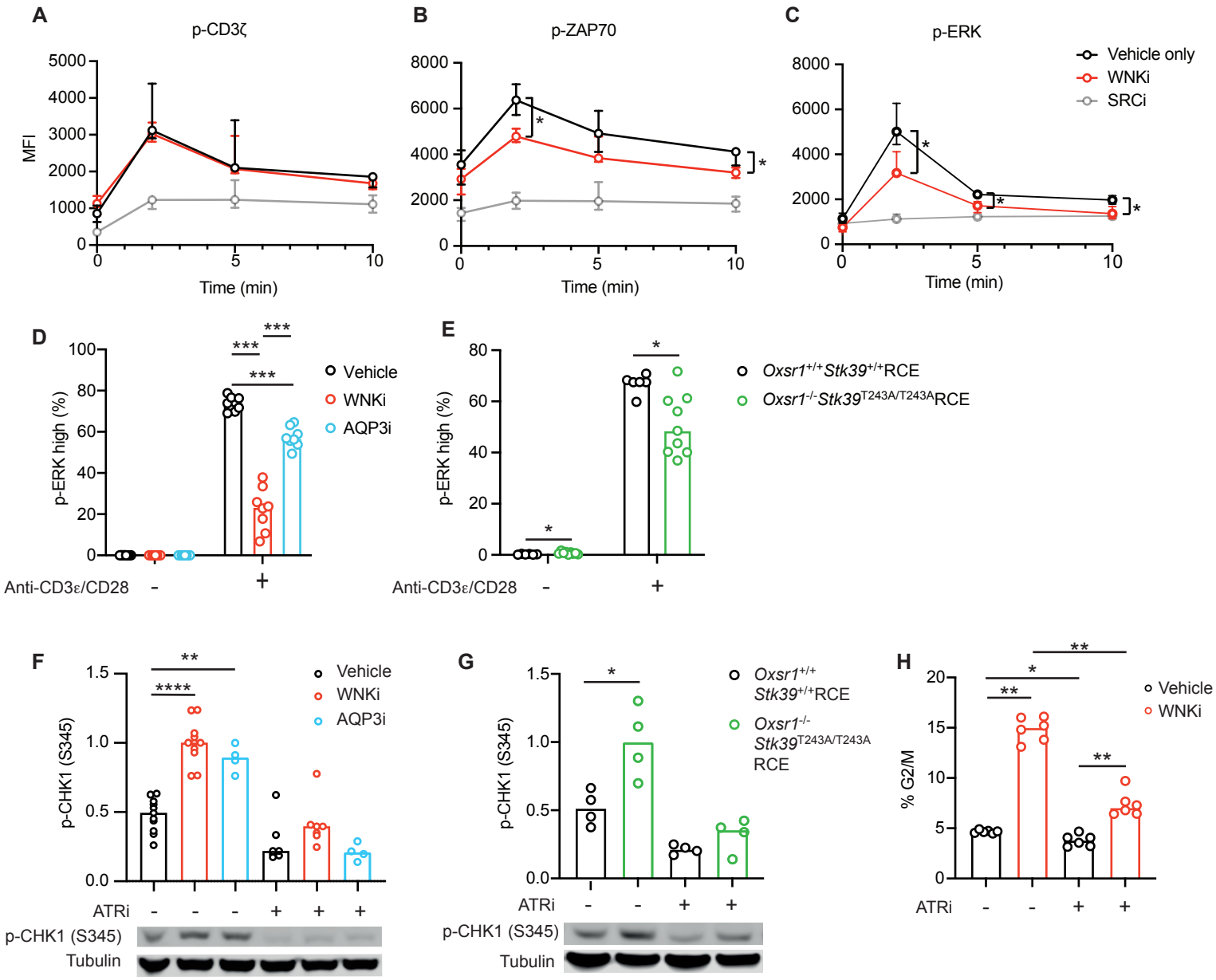
A
p-CD3ζ
MFI
Time (min)
B
p-ZAP70
Time (min)
C
p-ERK
Vehicle only
WNKi
SRCi
Time (min)
D
p-ERK high (%)
Vehicle
WNKi
AQP3i
Anti-CD3ε/CD28
E
p-ERK high (%)
Oxsr1+/+Stk39+/+RCE
Oxsr1-/-Stk39T243A/T243ARCE
Anti-CD3ε/CD28
F
p-CHK1 (S345)
Vehicle
WNKi
AQP3i
ATRi
p-CHK1 (S345)
Tubulin
G
p-CHK1 (S345)
Oxsr1+/+ Stk39+/+RCE
Oxsr1-/- Stk39T243A/T243A RCE
ATRi
p-CHK1 (S345)
Tubulin
H
% G2/M
Vehicle
WNKi
ATRi

Figure 5

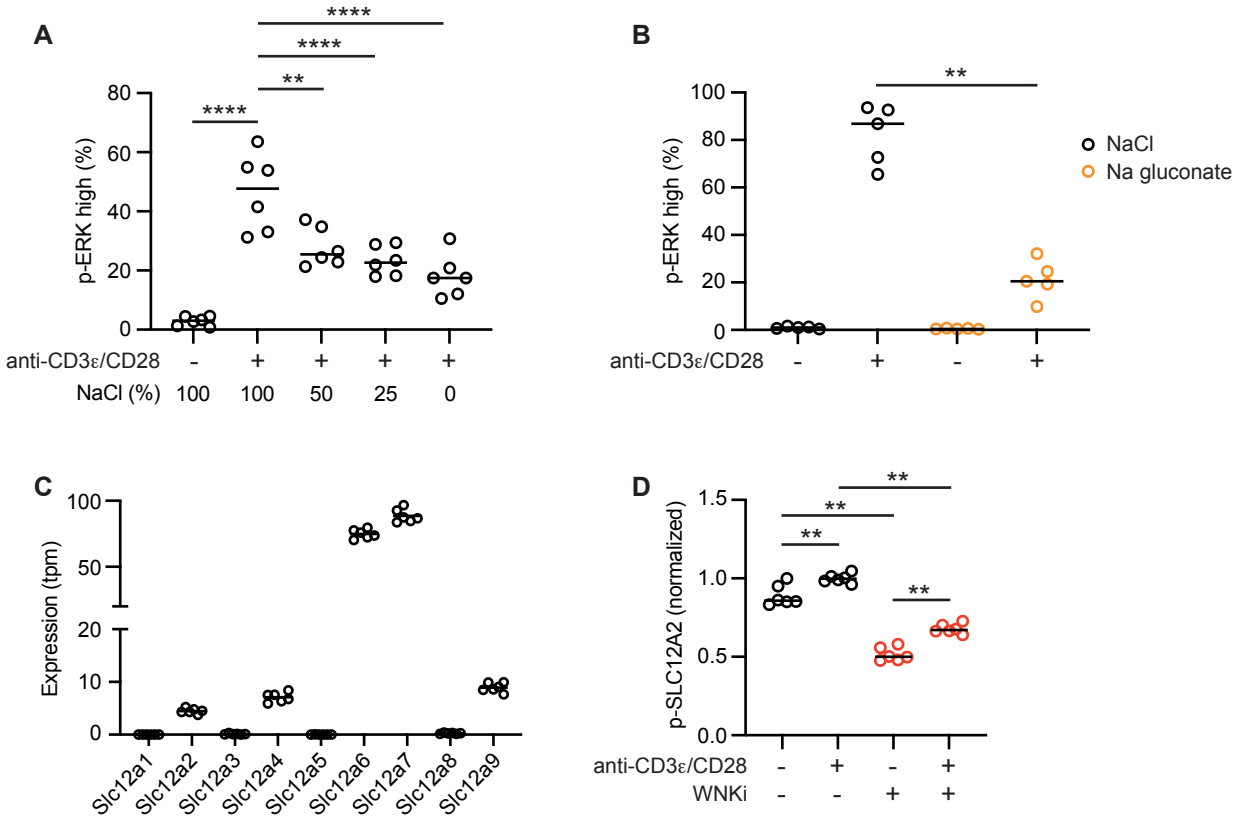
A
p-ERK high (%)
80
60
40
20
0
****
****
**
****
anti-CD3ε/CD28 - + + + +
NaCl (%) 100 100 50 25 0
B
p-ERK high (%)
100
80
60
40
20
0
**
anti-CD3ε/CD28 - + - +
NaCl
Na gluconate
C
Expression (tpm)
100
50
20
10
0
Slc12a1
Slc12a2
Slc12a3
Slc12a4
Slc12a5
Slc12a6
Slc12a7
Slc12a8
Slc12a9
D
p-SLC12A2 (normalized)
1.5
1.0
0.5
0.0
**
**
**
**
anti-CD3ε/CD28 - + - +
WNKi - - + +

Figure 6

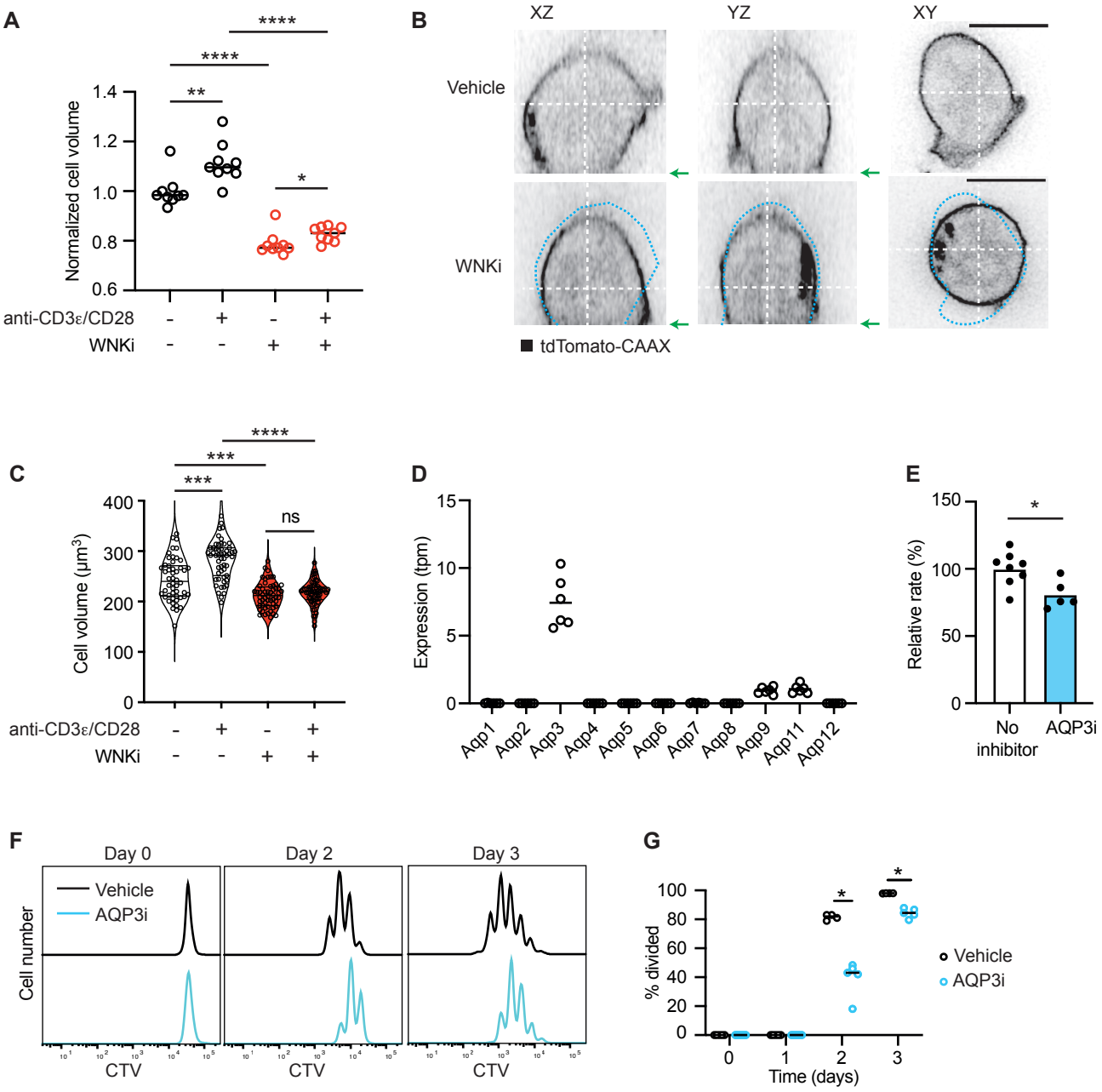
A
Normalized cell volume
1.4
1.2
1.0
0.8
0.6
****
****
**
*
anti-CD3ε/CD28 - + - +
WNKi - - + +
B
XZ
YZ
XY
Vehicle
WNKi
tdTomato-CAAX
C
Cell volume (μm³)
400
300
200
100
0
****
***
***
ns
anti-CD3ε/CD28 - + - +
WNKi - - + +
D
Expression (tpm)
15
10
5
0
Aqp1
Aqp2
Aqp3
Aqp4
Aqp5
Aqp6
Aqp7
Aqp8
Aqp9
Aqp11
Aqp12
E
Relative rate (%)
150
100
50
0
*
No inhibitor
AQP3i
F
Day 0
Day 2
Day 3
Vehicle
AQP3i
Cell number
CTV
CTV
CTV
G
% divided
100
80
60
40
20
0
*
*
0
1
2
3
Time (days)
Vehicle
AQP3i

Figure 7

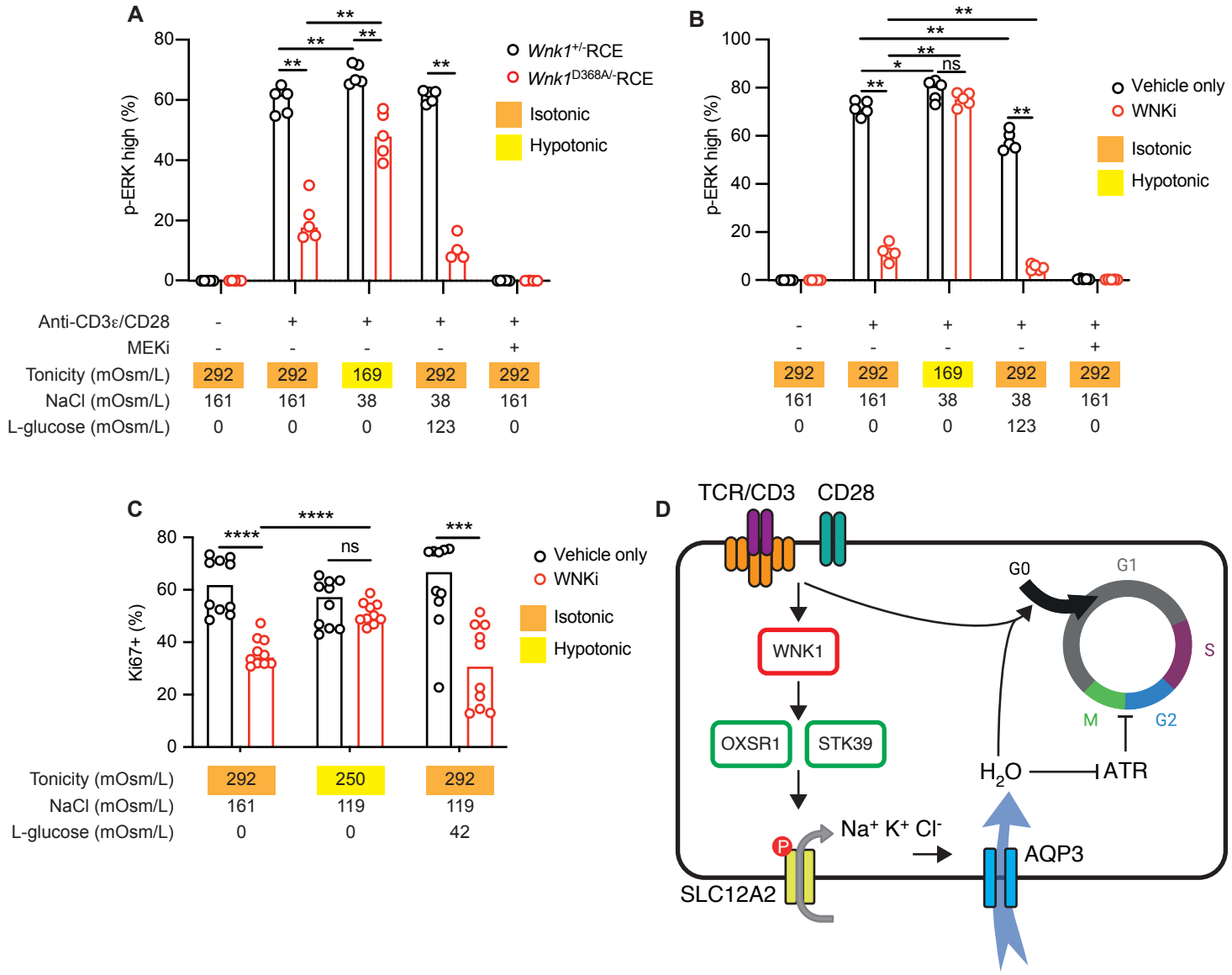
A
p-ERK high (%)
80
60
40
20
0
**
**
**
**
**
Wnk1+/-RCE
Wnk1D368A/-RCE
Isotonic
Hypotonic
Anti-CD3ε/CD28 - + + + +
MEKi - - - - +
Tonicity (mOsm/L) 292 292 169 292 292
NaCl (mOsm/L) 161 161 38 38 161
L-glucose (mOsm/L) 0 0 0 123 0
B
p-ERK high (%)
100
80
60
40
20
0
**
**
**
*
ns
**
**
Vehicle only
WNKi
Isotonic
Hypotonic
- + + + +
- - - - +
292 292 169 292 292
161 161 38 38 161
0 0 0 123 0
C
Ki67+ (%)
80
60
40
20
0
****
****
ns
***
Vehicle only
WNKi
Isotonic
Hypotonic
Tonicity (mOsm/L) 292 250 292
NaCl (mOsm/L) 161 119 119
L-glucose (mOsm/L) 0 0 42
D
TCR/CD3
CD28
WNK1
OXSR1
STK39
P
SLC12A2
Na+ K+ Cl-
AQP3
H2O
ATR
G0
G1
S
G2
M

Water influx is required for CD4$^+$ T cell activation and T cell-dependent antibody responses

Supplementary Information

Supplementary Table 1. Antibodies used in this study.

Antigen	Clone	Supplier	Dilution
ERK	3A7	Cell Signaling Technology	1:1000 (Immunoblot)
OXSR1	Polyclonal	MRC PPU Reagents and services	1:1000 (Immunoblot)
p-CHK1 (S345)	133D3	Cell Signaling Technology	1:1000 (Immunoblot)
p-OXSR1 (S325)	Polyclonal	MRC PPU Reagents and Services	1:1000 (Immunoblot)
p-RPA32 (S4/8)	Polyclonal (#A300-245A)	Bethyl Laboratories	1:1000 (Immunoblot)
α-Tubulin	TAT-1	Cell Services STP, Crick	1:15000 (Immunoblot)
γH2AX (S139)	JBW301	Merck Millipore	1:10000 (Immunoblot)
Mouse IgG	IRDye® 800CW	LI-COR Biosciences	1:4000 (Immunoblot)
Mouse IgG	Alexa Fluor 680	ThermoFisher	1:4000

		Scientific	(Immunoblot)
Rabbit IgG	IRDye® 800CW	LI-COR Biosciences	1:4000 (Immunoblot)
Rabbit IgG	Alexa Fluor 680	ThermoFisher Scientific	1:4000 (Immunoblot)
Sheep IgG	Alexa Fluor 680	ThermoFisher Scientific	1:4000 (Immunoblot)
CD3ε	145-2C11	Tonbo Biosciences	1:125 (plate-bound stimulation) 1:50 (soluble stimulation)
CD28	37.51	Biolegend	1:250 (plate-bound stimulation) 1:100 (soluble stimulation)
Hamster IgG (H&L chain)	Polyclonal (#ABIN101378)	Antibodies-online.com	1:25 (soluble stimulation)
CD4	GK1.5	ThermoFisher Scientific	1:200 (FACS)
CD45.1	A20	ThermoFisher Scientific	1:100 (FACS)
CD45.2	104	Biolegend	1:100 (FACS)
CXCR5	2G8	BD Biosciences	1:100 (FACS)
Ki67	SolA15	ThermoFisher Scientific	1:100 (FACS)

p-CD3ξ (Y142)	K25-407.69	BD Biosciences	1:400 (1.25 µg/mL) (FACS)
p-ERK1 (T202/Y204)	Polyclonal (#9101)	Cell Signaling Technology	1:50 (FACS)
p-ERK2 (T185/Y187)	Polyclonal (#9101)	Cell Signaling Technology	1:50 (FACS)
p-MPM2 (S/TP motif)	MPM-2	Merck Millipore	1:100 (FACS)
p-ZAP-70 (Y319)	65E4	Cell Signaling Technology	1:400 (FACS)
p-SLC12A2 (T203/T207/T212)	Polyclonal	MRC PPU	1:200 (FACS)
PD-1	29F.1A12	Biolegend	1:100 (FACS)
Mouse IgG (H&L chain)	Donkey polyclonal (highly cross-adsorbed) – AF488	ThermoFisher Scientific	1:500 (FACS)
Rabbit IgG (H&L chain)	Goat polyclonal (highly cross-adsorbed) – AF647	ThermoFisher Scientific	1:500 (FACS)
Sheep IgG	Donkey Polyclonal (highly cross-adsorbed) – CF647	Biotium	1:500 (FACS)
Streptavidin	APC	ThermoFisher Scientific	1:500 (FACS)

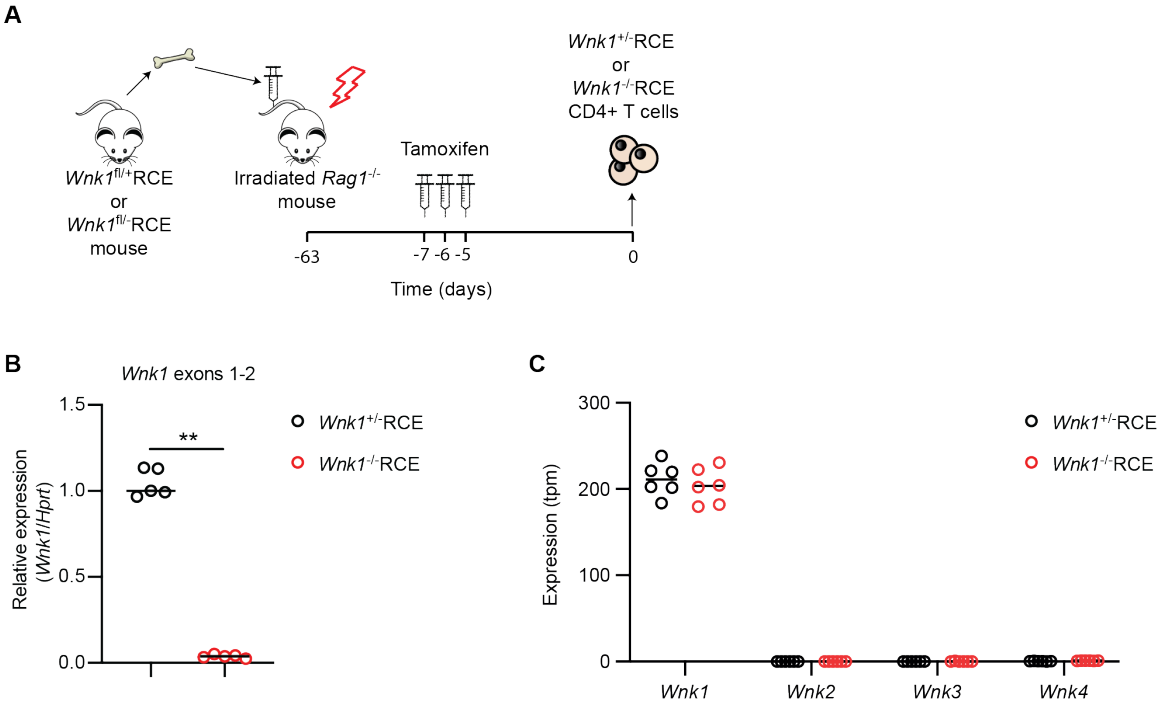

Supplementary Figure 1. Generation of WNK1-deficient T cells.

(**A**) Bone marrow from *Wnk1*$^{fl/+}$/RCE and *Wnk1*$^{fl/-}$/RCE mice was transferred into irradiated RAG1-deficient mice. At least 8 weeks later, the chimeras were treated with tamoxifen on three successive days. Lymph nodes were harvested 7 d after start of tamoxifen treatment and WNK1-expressing (*Wnk1*$^{+/-}$RCE) or WNK1-deficient (*Wnk1*$^{-/-}$RCE) naive CD4^{+} T cells purified. (**B**) Graph of qPCR measurement of mRNA levels of *Wnk1* (exons 1-2) relative to *Hprt* in *Wnk1*$^{+/-}$RCE and *Wnk1*$^{-/-}$RCE naïve CD4^{+} T cells generated as in A, normalized to median level in *Wnk1*$^{+/-}$RCE T cells which was set to 1 (n = 5). (**C**) mRNA levels of *Wnk* genes in *Wnk1*$^{+/-}$RCE and *Wnk1*$^{-/-}$RCE CD4^{+} T cells determined by RNAseq; tpm, transcripts per million reads (n=6). Note that while exon 2 of *Wnk1* is efficiently deleted in *Wnk1*$^{-/-}$RCE CD4^{+} T cells, as shown in B, the remaining 27 exons are intact and still expressed, which is why the total amount of *Wnk1* mRNA is not decreased in the *Wnk1*$^{-/-}$ RCE cells. The deletion of exon 2 from the *Wnk1* transcript removes part of the kinase domain and results in a frameshift, so the mutant allele destroys kinase activity and is most likely a null. Each point represents a different mouse; horizontal lines show median;

data pooled from 1 (C) or 2 (B) independent experiments. Statistical analysis carried out using the Mann-Whitney U test. ** $0.001 < p < 0.01$.

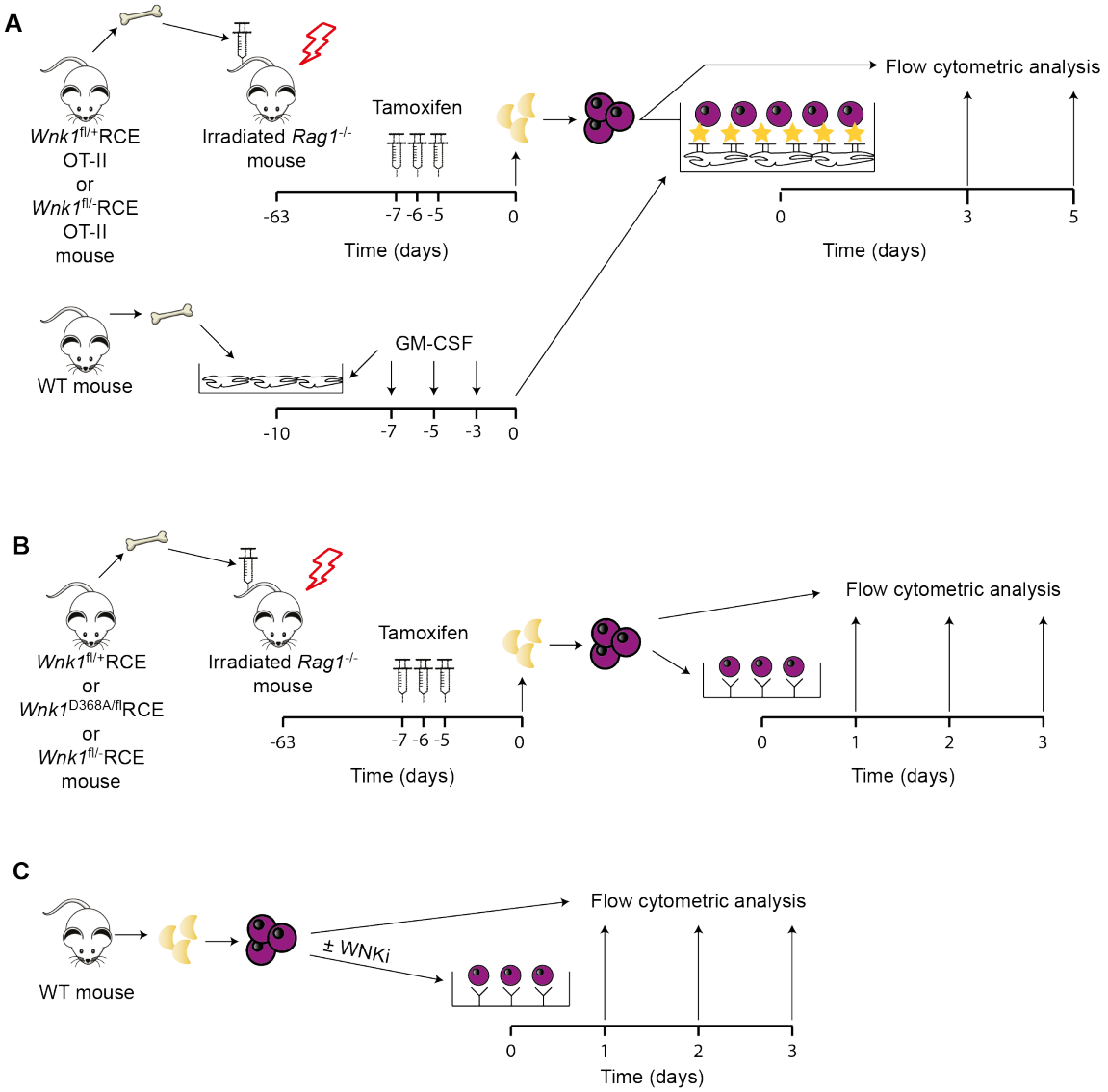

Supplementary Figure 2. *In vitro* analysis of activation of WNK1-deficient CD4$^+$ T cells.

(**A**) Bone marrow from *Wnk1*$^{fl/+}$RCE OT-II and *Wnk1*$^{fl/-}$RCE OT-II mice was transferred into irradiated RAG1-deficient mice. At least 8 weeks later, the chimeras were treated with tamoxifen on three successive days to delete the floxed exon 2 of *Wnk1*, lymph nodes harvested 7 d after start of tamoxifen treatment and WNK1-expressing (*Wnk1*$^{+/-}$RCE OT-II) or WNK1-deficient (*Wnk1*$^{-/-}$RCE OT-II) naive CD4$^+$ T cells purified. APCs were generated from WT bone marrow cells cultured in GM-CSF containing medium for 10 d.

T cells were labelled with CTV and co-cultured with APCs for up to 5 days, in the presence of indicated concentrations of $OVA_{323-339}$ peptide and analyzed by flow cytometry. (**B**) Bone marrow from *Wnk1*$^{fl/+}$RCE, *Wnk1*$^{fl/-}$RCE or *Wnk1*$^{D368A/fl}$RCE mice was transferred into irradiated RAG1-deficient mice. At least 8 weeks later, the chimeras were treated with tamoxifen on three successive days, lymph nodes harvested 7 d after start of tamoxifen treatment and WNK1-expressing (*Wnk1*$^{+/-}$RCE), WNK1-deficient (*Wnk1*$^{-/-}$RCE) or WNK1-D368A expressing (*Wnk1*$^{D368A/-}$RCE) naive $CD4^+$ T cells were purified. T cells were labelled with CTV and activated using plate-bound anti-CD3ε and anti-CD28 antibodies and analyzed by flow cytometry up to 3 d later. (**C**) WT naïve $CD4^+$ T cells were labelled with CTV, activated on anti-CD3ε and anti-CD28 antibodies in the presence or absence of WNKi and analyzed at indicated time points. WNKi, WNK inhibitor (WNK463).

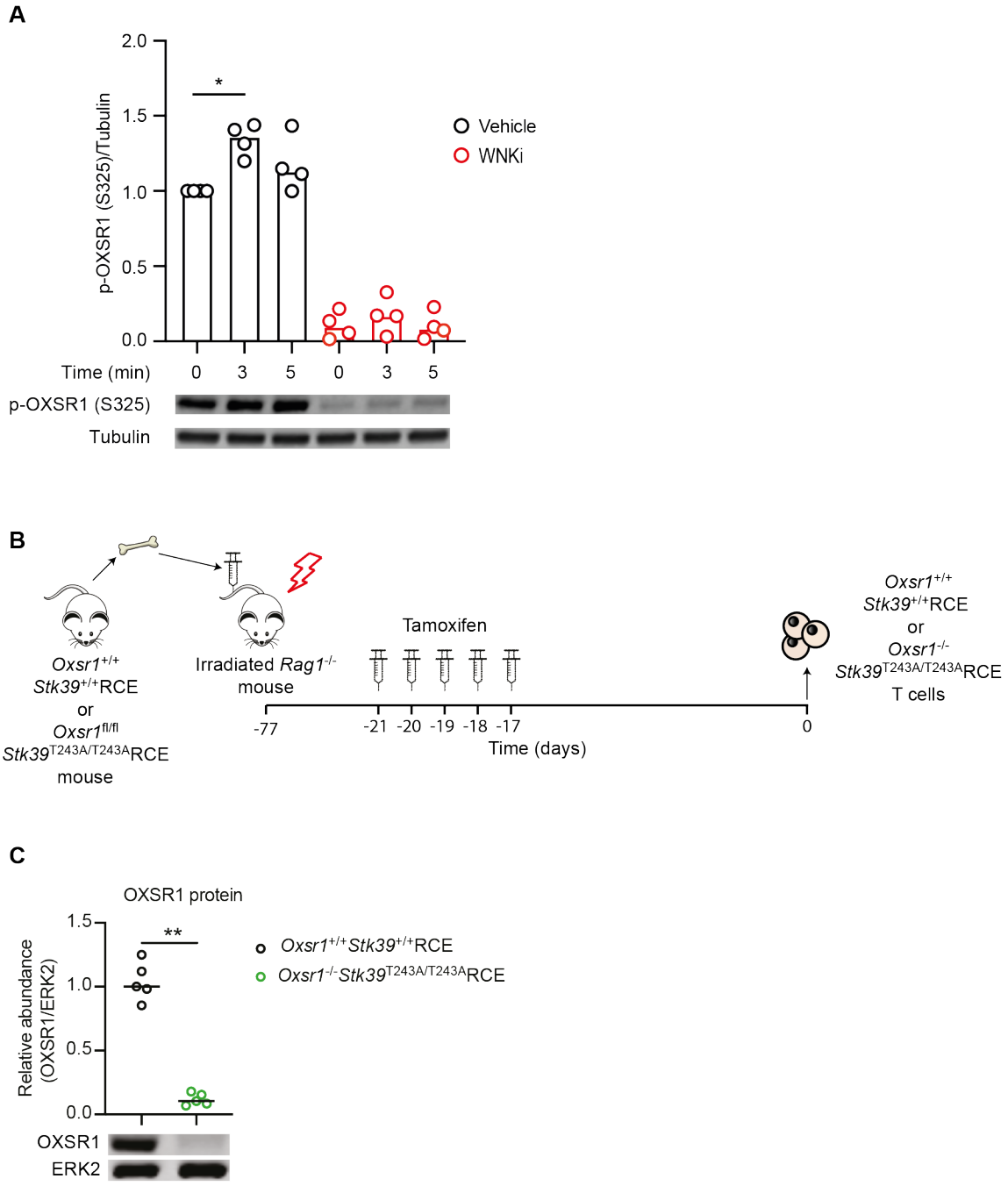

Supplementary Figure 3. Generation of CD4⁺ T cells with mutations in both *Oxsr1* and *Stk39*.

(**A**) Graph and example immunoblot of p-OXSR1 (S325) and tubulin from lysates of naïve CD4⁺ T cells stimulated by cross-linking soluble anti-CD3ε and anti-CD28 antibodies for indicated timepoints (n=4). Data normalised to vehicle-treated sample at time 0 min which

was set to 1. WNKi, WNK inhibitor (WNK463). (**B**) Bone marrow from *Oxsr1*$^{+/+}$*Stk39*$^{+/+}$RCE and *Oxsr1*$^{fl/fl}$*Stk39*$^{T243A/T243A}$RCE mice was transferred into irradiated RAG1-deficient mice. At least 8 weeks later, the chimeras were treated with tamoxifen on five successive days to delete the floxed exons 9 and 10 of *Oxsr1*, lymph nodes harvested 21 d after start of tamoxifen treatment and *Oxsr1*$^{+/+}$*Stk39*$^{+/+}$RCE or *Oxsr1*$^{-/-}$*Stk39*$^{T243A/T243A}$RCE naive CD4^{+} T cells purified. (**C**) Abundance of OXSR1 in *Oxsr1*$^{+/+}$*Stk39*$^{+/+}$RCE or *Oxsr1*$^{-/-}$ *Stk39*$^{T243A/T243A}$RCE CD4^{+} T cells was determined by immunoblotting total cell lysates for OXSR1 and ERK2 and normalizing the ratio of OXSR1 to ERK2 to the median value in *Oxsr1*$^{+/+}$*Stk39*$^{+/+}$RCE T cells which was set to 1 (example immunoblot shown below graph) (n = 5). Each point represents a different mouse; horizontal lines or columns indicate median; data shown from 1 experiment representative of 2 independent experiments (C) or pooled from 3 independent experiments (A). Statistical analysis carried out using the Mann-Whitney U test; * $p<0.05$, ** $0.001 < p < 0.01$.

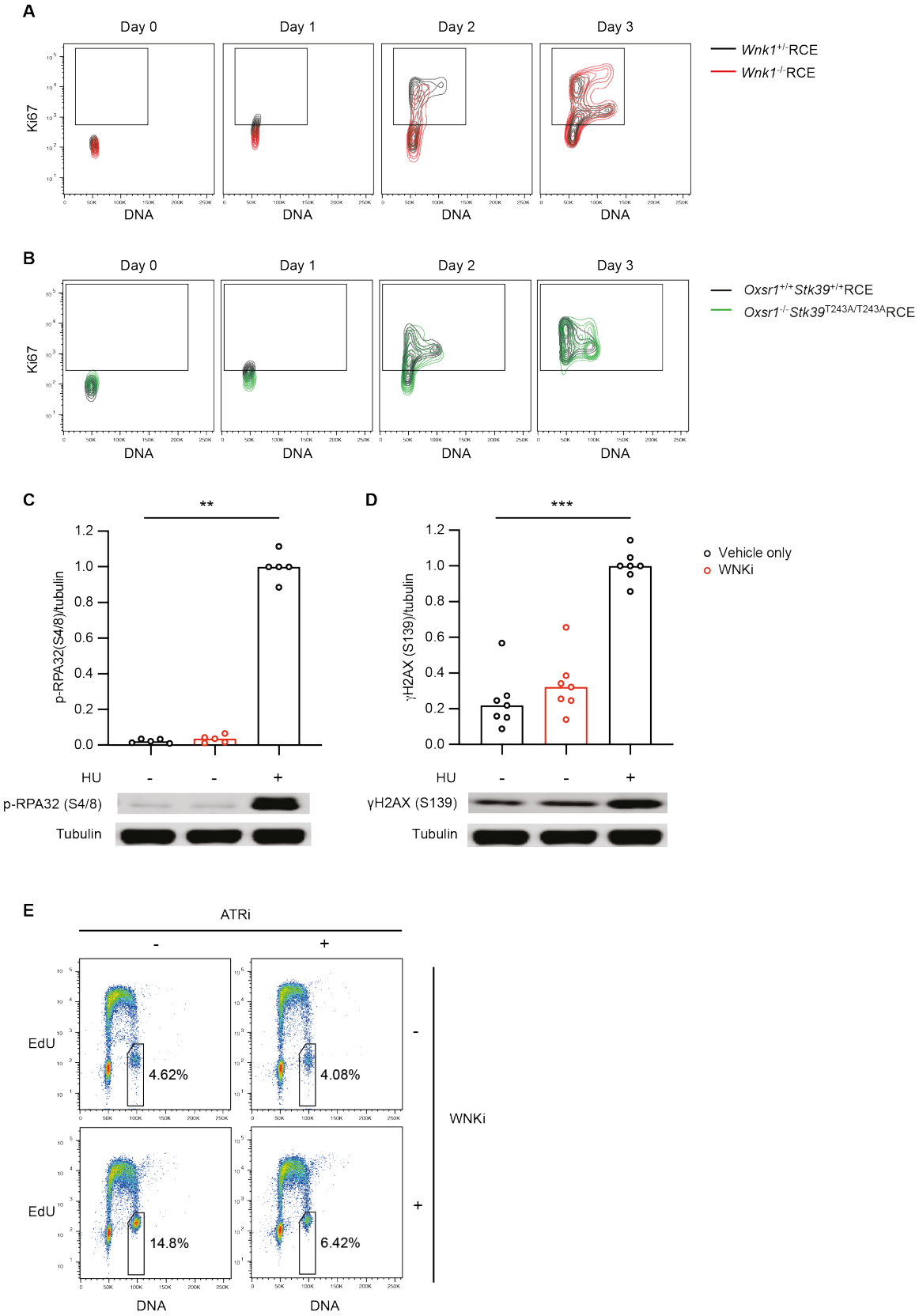
A
Day 0
Day 1
Day 2
Day 3
Ki67
DNA
Wnk1+/-RCE
Wnk1-/-RCE
B
Oxsr1+/+Stk39+/+RCE
Oxsr1-/-Stk39T243A/T243ARCE
C
**
p-RPA32(S4/8)/tubulin
HU
p-RPA32 (S4/8)
Tubulin
D
***
γH2AX (S139)/tubulin
γH2AX (S139)
Vehicle only
WNKi
E
ATRi
EdU
4.62%
4.08%
14.8%
6.42%
WNKi

Supplementary Figure 4. Delayed TCR/CD28-induced entry into G1 in CD4$^+$ T cells with mutations in *Wnk1*, *Oxsr1* and *Stk39*.

(**A, B**) Example flow cytometric density plots of Ki67 expression and DNA content of CD4$^+$ T cells of the indicated genotypes activated on plate-bound anti-CD3ε and anti-CD28 antibodies for the indicated times. Gates show Ki67$^+$ populations used to generate data in Figures 3A, F. (**C**, **D**) Graphs showing abundance of p-RPA32 (S4/S8) (C) and γH2AX (S139) (D) relative to Tubulin in CD4$^+$ T cells activated on plate-bound anti-CD3ε and anti-CD28 antibodies for 3 d in the presence of WNKi or vehicle only (n=5-7). Where indicated, 4 mM hydroxyurea (HU) was added for the final 2 h of culture. Amounts of p-RPA32 and γH2AX were determined by immunoblotting total cell lysates with antibodies to these phosphorylated proteins and to Tubulin and normalizing the resulting pRPA32/tubulin and γH2AX/tubulin ratios to the median ratio in HU-treated cells which was set to 1. Columns show median; each point represents a single mouse. (**E**) Representative flow cytometric pseudocolor plots of DNA and EdU content of single, live CD4$^+$ T cells activated for 72 h on anti-CD3ε- and anti-CD28-coated cell culture dishes. Cells were treated with WNKi for 72 h or ATRi for 6 h where indicated and pulsed with EdU for the final 30 min of the culture. Gates indicate cells in G2/M used to generate data in Figure 4H, numbers indicate percentage of cells falling into the gate. Data pooled from 3 independent experiments (C, D). Statistical analysis carried out using Mann-Whitney U test. ** $0.001 < p < 0.01$; ***$0.0001<p<0.001$.

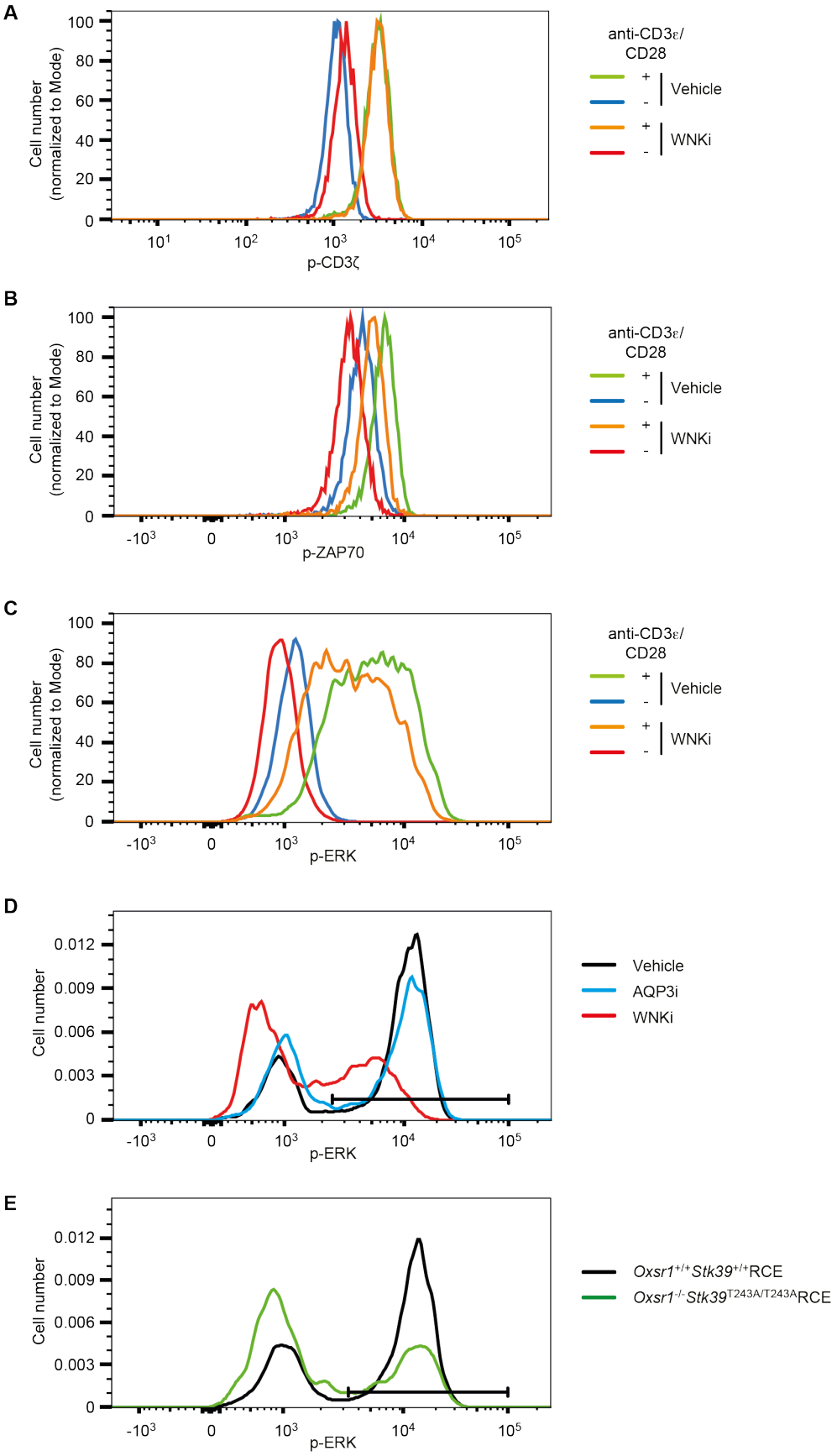
A
Cell number (normalized to Mode)
p-CD3ζ
anti-CD3ε/ CD28
+
-
Vehicle
+
-
WNKi
B
Cell number (normalized to Mode)
p-ZAP70
anti-CD3ε/ CD28
Vehicle
WNKi
C
Cell number (normalized to Mode)
p-ERK
anti-CD3ε/ CD28
Vehicle
WNKi
D
Cell number
p-ERK
Vehicle
AQP3i
WNKi
E
Cell number
p-ERK
Oxsr1+/+Stk39+/+RCE
Oxsr1-/-Stk39T243A/T243ARCE

Supplementary Figure 5. Flow cytometric analysis of early TCR signaling.

(**A-E**) Example flow cytometric histograms of intracellular staining with antibodies for p-CD3ζ (Y142) (A), p-ZAP70 (Y319) (B), and p-ERK1/2 (T202/Y204) (C-E) of $CD4^+$ T cells that had been activated or not with soluble anti-CD3ε and anti-CD28 antibodies for 2 min (A-C) or with plate-bound antibodies for 1 h (D, E). Cells were treated with inhibitors as indicated. Cells were from C57BL/6J mice (A-D) or were of the indicated genotypes (E). Gating for p-ERK high cells is shown (D, E). WNKi, WNK inhibitor (WNK463); AQP3i, AQP3 inhibitor (DFP00173).

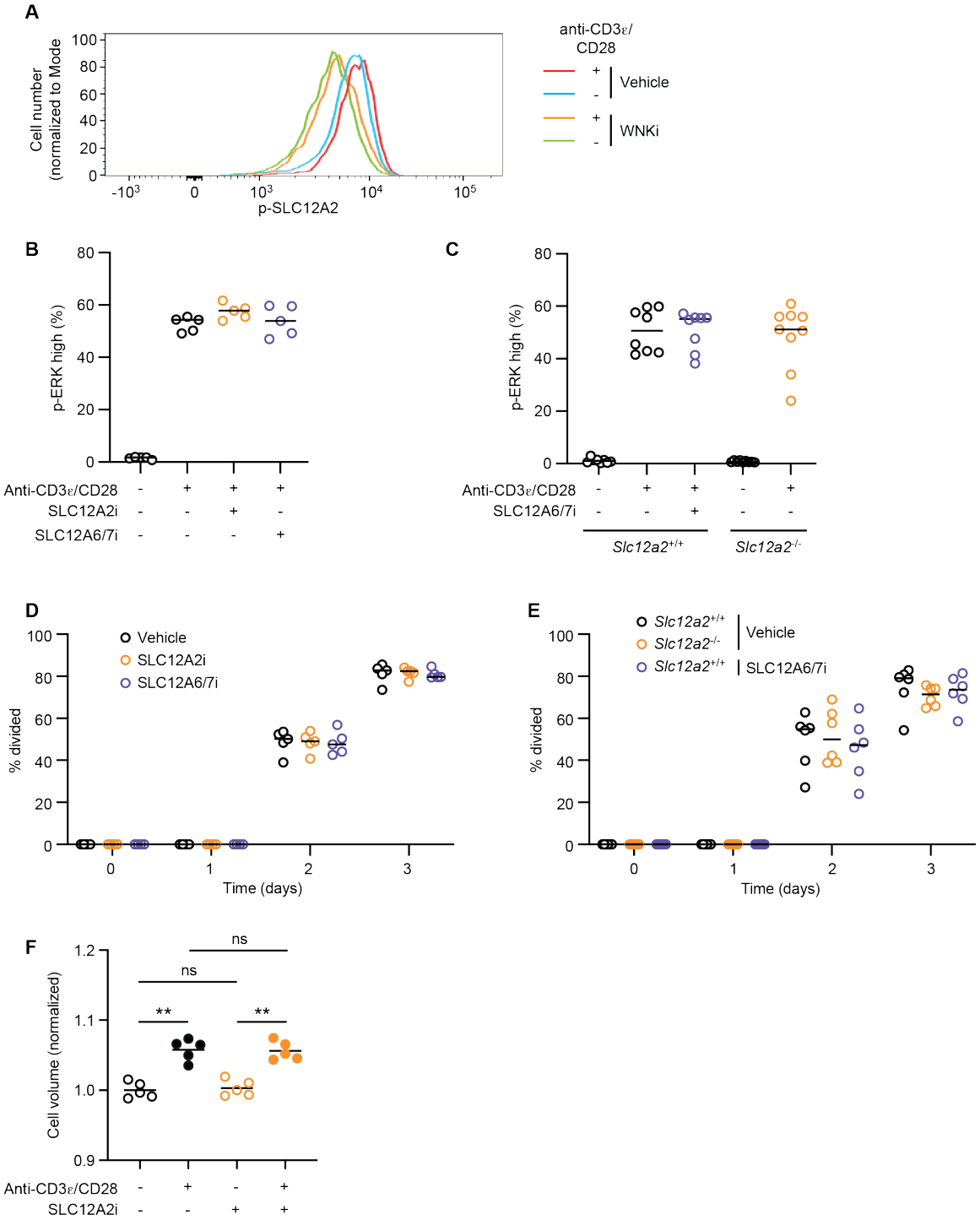

Supplementary Figure 6. SLC12A2, SLC12A6 and SLC12A7 are not required for TCR-induced activation or proliferation.

(**A**) Example flow cytometric histograms of intracellular staining with an antibody for p-SLC12A2 (T203/T207/T212) in CD4$^+$ T cells that had been activated or not with plate-

bound antibodies for 1 h in the presence or absence of WNKi. (**B-C**) Percentage of p-ERK high $CD4^+$ T cells that had been activated or not with plate-bound antibodies for 1 h in the presence or absence of inhibitors. Cells were from C57BL/6J mice (B) or of the indicated genotypes (C) (n=6-9). (**D-E**) CTV-labelled $CD4^+$ T cells were incubated with plate-bound antibodies for the indicated times and CTV dilution was used to determine the percentage of cells that had divided at least once (n=6). (**F**) Volume of naïve WT $CD4^+$ T cells activated for 1 h in the presence of vehicle only or SLC12A2i on plate-bound anti-CD3ε and anti-CD28 antibodies where indicated, determined using a Casy® cell counter and normalized to the mean volume of cells in the absence of stimulation or inhibitor. Each dot represents the modal volume of ≥200 cells (n = 5). WNKi, WNK inhibitor (WNK463); SLC12A2i, SLC12A2 inhibitor (bumetanide); SLC12A6/7i, SLC12A6 and SLC12A7 inhibitor (DIOA). Dots represent cells from a single mouse, lines indicate median (B-E) or mean (F). Data pooled from 2 (B-E) or 1 (F) independent experiments. Statistical analysis with a Mann-Whitney test showed that SLC12A2i and SLC12A6/7i and the genetic loss of *Slc12a2* had no significant effect on the percentage of p-ERK high cells or the percentage of cells that had divided. ** $0.001 < p < 0.01$; ns, not significant.

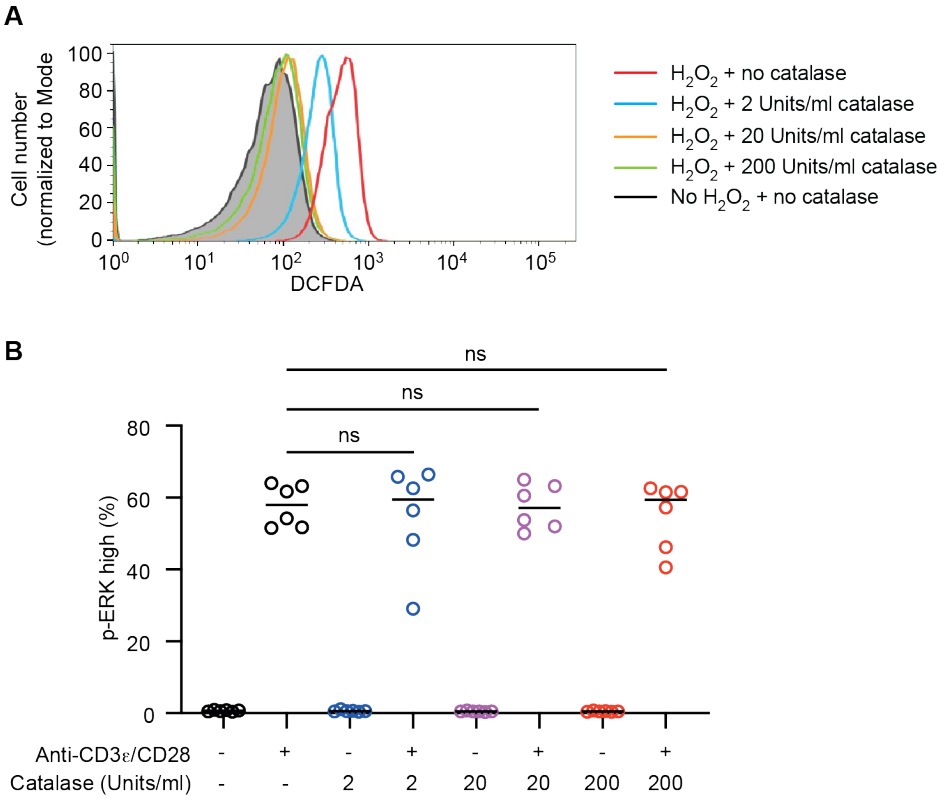

Supplementary Figure 7. Extracellular H_2O_2 is not required for TCR-induced activation.

(**A**) Representative flow cytometry plot of mouse naïve $CD4^+$ T cells stained with the reactive oxygen species indicator DCFDA, pre-incubated with catalase at the indicated concentrations. Where indicated, cells were treated with 1 mM H_2O_2 for 30 min and analyzed using flow cytometry. (**B**) $CD4^+$ T cells were activated on plate-bound anti-CD3ε and anti-CD28 antibodies for 1 h, as indicated, in the presence of different concentrations of catalase. Graph shows percentage p-ERK high cells (n=6). Data pooled from 2 experiments (B). Statistical analysis with a Mann-Whitney test showed that catalase had no significant effect (ns) on the percentage of p-ERK high cells.

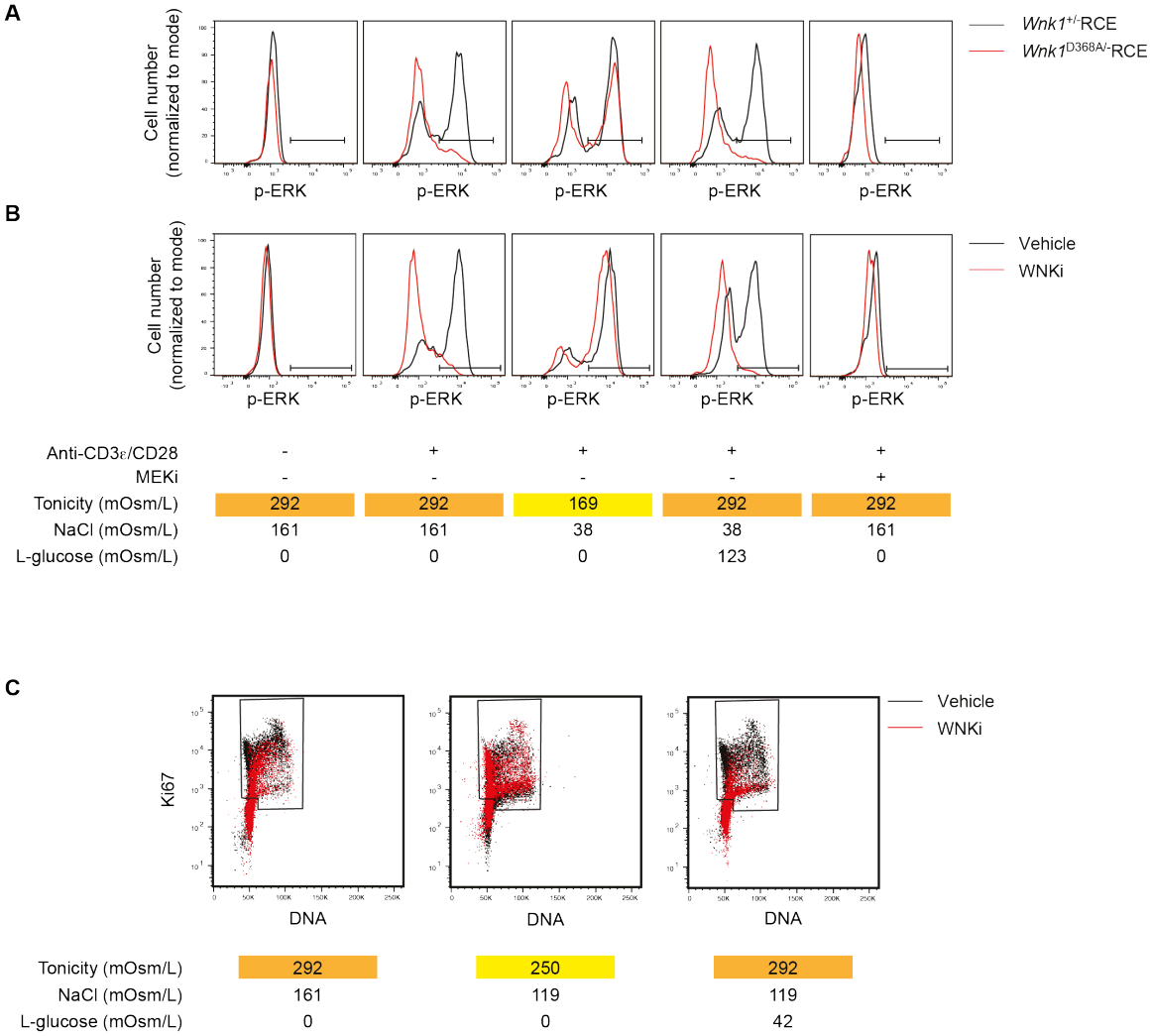

Supplementary Figure 8. WNK1-dependent water influx is required for TCR signaling and G1 entry.

(**A**, **B**) Histograms of phospho-ERK1/2 (p-ERK, T202/Y204) abundance in CD4$^+$ T cells activated for 1 h on plates coated with anti-CD3ε and anti-CD28 antibodies at the tonicities indicated and in the presence of MEKi or vehicle only, measured by flow cytometry. Histograms show a comparison of *Wnk1*$^{+/-}$RCE and *Wnk1*$^{D368A/-}$RCE CD4$^+$ T cells (A) or WT CD4$^+$ T cells treated with WNKi or vehicle (B). Gate indicates p-ERK high cells. (**C**) Example dot plots of Ki67 expression and DNA content of WT CD4$^+$ T cells activated for 2 d on anti-CD3ε and anti-CD28 antibodies in the presence of WNKi or vehicle only at the

tonicities indicated, made by altering NaCl and L-glucose concentrations, measured by flow cytometry; gate indicates Ki67^{+} cells, excluding Ki67^{-} cells in G0. WNKi, WNK inhibitor (WNK463).